Geomorphic expressions of active rifting reflect the role of structural inheritance: A new model for the evolution of the Shanxi Rift, North China

Malte Froemchen[1], Ken J. W. McCaffrey[1], Mark B. Allen[1], Jeroen van Hunen[1], Thomas B. Phillips[1], Xu Yueren[2]

[1]Department of Earth Sciences, Durham University, Science Labs, Durham, DH13LE, UK
[2]Key Laboratory of Earthquake Prediction, Institute of Earthquake Forecasting, China Earthquake Administration, Beijing, China

Correspondence to: Malte Froemchen (malte.froemchen@durham.ac.uk)

Abstract. Many rifts are influenced by pre-existing structures and heterogeneities during their evolution, a process known as structural inheritance. During rift evolution, these heterogeneities may aid rift nucleation, growth, and segmentation of faults, encourage linkage of various segments, or even inhibit the formation of faults. Understanding how structural inheritance influences early rift evolution could be vital for evaluating seismic risk in tectonically active areas. The Shanxi Rift in the north of China is an active rift system believed to have formed along the trend of the Proterozoic Trans North China Orogen, however, the influence of these pre-existing structures on the present-day rift architecture is poorly known. Here we use tectonic geomorphological techniques, e.g., hypsometric integral (HI), channel steepness (k_{sn}) and local relief to study the evolution of the Shanxi Rift and identify areas of higher tectonic activity. We found that HI was less sensitive to lithology and more valuable in evaluating the tectonic signal and found that activity is concentrated in two rift interaction zones (RIZ) formed between the basins. We then evaluate the relationship between the active faults and mapped pre-existing structures and found that many faults formed parallel to inherited structures but faults in the RIZs often crosscut these structures. Based on these observations we propose a new model for the evolution of the Shanxi Rift where inherited structures play an important part in the initial segmentation of the rift which in turn controls the development of the RIZ structures.

1 Introduction

Many continental rifts exploit ancient orogenic belts to accommodate extensional strain. Examples include East African Rift (Rosendahl, 1987; Morley, 1988; Ring, 1994), Baikal Rift (Petit et al., 1996), and the Rhine Graben (Schuhmacher, 2002). Research has focused on understanding the relationship between old pre-rift structures and how they control the development of younger structures. Pre-existing orogenic belts influence the accommodation of subsequent episodes of extensional strain, due to the presence of discrete and mechanically weak structures, such as shear zones and associated metamorphic fabrics (McCaffrey, 1997; Phillips et al., 2016, Fazlikhani et al., 2017; Kolawole et al., 2018; Peace et al., 2018; Heilman et al., 2019), pre-existing fault networks (Holdsworth et al., 2001) or lithological contacts (Wedmore et al., 2020; Phillips and McCaffrey,

2019). These mechanical strength contrasts are particularly significant where orogenic belts are adjacent to cratons (Dunbar and Sawyer, 1988; Ziegler and Cloethingh, 2004; Corti et al. 2013) as is the case for the Baikal Rift (Petit et al. 1996), the East

35 African Rift (Versfelt and Rosendahl, 1989) and the Circum-Ordos rifts in North China (Xu and Ma, 1992; Su et al., 2021), because cratonic lithosphere is more resistant to deformation than younger orogenic belts.

Studies of the interaction between rift-related normal faults and inherited structures in offshore basins and margins use high resolution 2D and 3D seismic reflection data to analyse the influence of inheritance on spatiotemporal patterns of rift evolution (Morley et al., 2004; Phillips et al., 2016; Peace et al., 2018, Mulaya et al., 2022). Detailed field studies, on the other hand, can

40 resolve the kinematic response of faults and infer strainfield directions and interactions (e.g., East Africa, Hodge et al., 2018a; Wedmore et al., 2020; Heilman et al., 2019; Kolawole et al., 2018). Inherited structures and heterogeneities can influence the location, morphology, segmentation, and orientation of an entire rift zone (Wilson et al., 1966; Tommasi and Vauchez, 2001; Şengör et al., 2019; Heron et al., 2019; Schiffer et al., 2020; Kolawole et al. 2022). They can also influence the geometry and kinematics of individual faults (Wedmore et al., 2020; Samsu et al., 2020; Wilson et al., 2010). Inherited structures can

45 influence the development of rifts and their associated basins by controlling linkage of fault segments (Brune et al., 2017; Heilman et al., 2019). Inherited structures have also been shown to act as barriers to rift faults if they form structures or regions of strengthened crust that is harder to deform than surrounding areas (Krabbendam and Barr, 2000; Phillips and McCaffrey, 2019).

Many rifts that show a strong influence of inheritance are very segmented and exhibit numerous faults and basins that vary in

50 orientation and morphology (Morley et al., 2004; Reeve et al., 2015; Heron et al., 2019; Osagiede et al., 2020). Between individual basins of a rift zone a complex deformation zone known as Rift Interaction Zone (RIZ) may develop (Nelson et al., 1992; Koehn et al., 2008; Aanyu and Koehn, 2011; Sachau et al., 2016; Kolawole et al., 2021a). The morphology of these zones is principally controlled by the separation distance between fault segments, the polarity of the respective faults and the amount of overlap between them (Morley et al., 1990; Faulds and Varga, 1998; Zwaan and Schreurs, 2017, Zwaan et al., 2016).

55 Commonly, these zones are topographically distinct from the rest of the rift. RIZs may form topographic highs in their early evolution, forming as a drainage divide between depocenters (Ebinger et al., 1987; Lambiase and Bosworth, 1995; Gawthrope & Hurst, 1993) and therefore acting as a source of sediment (Gawthrope and Hurst, 1993; Scholz, 1995). As RIZs evolve, they can become breached and eventually link up the rift basins (Kolawole et al., 2021a). RIZs may also show a perturbated local strain field due to the influence of the adjacent, bounding rift faults (Crider and Pollard, 1998; Kattenhorn et al., 2000; Maerten,

60 2000; Kolawole et al., 2024). Development of these zones may be aided by basement fabrics that strike oblique to the main extension direction (Fossen and Rotevatn, 2016); however, basement fabrics may also influence linkage across these zones (Morley et al., 2004; Heilman et al., 2019; Kolawole et al., 2021a). RIZs are important structural domains along rift systems, and inheritance may be key to understanding their geometry and evolution.
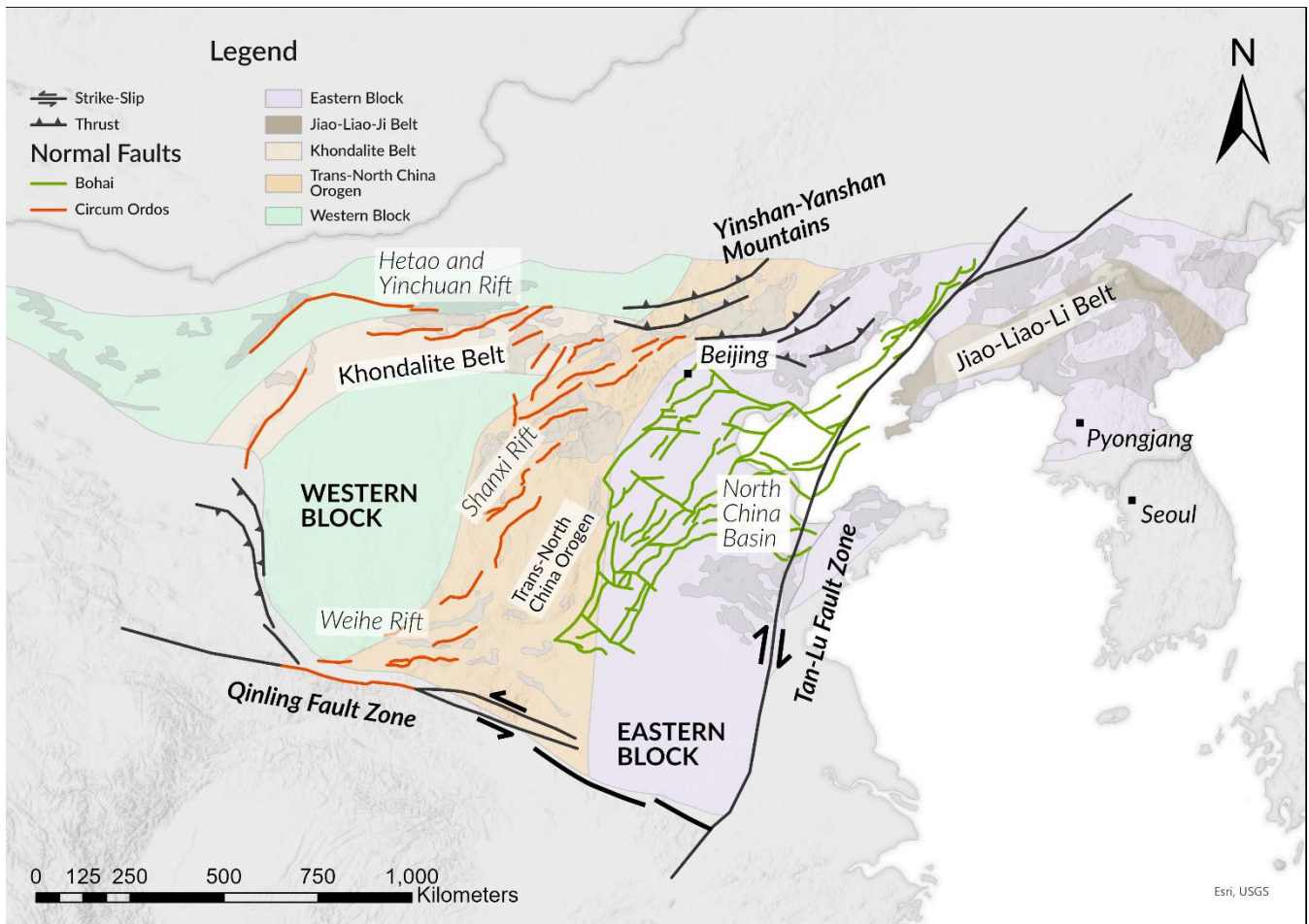
Figure 1: Overview map of the North China Craton (NCC) with boundaries of the different blocks and orogenic belts that make up the NCC shaded in colour. Boundaries after Zhao et al. 2005. Also indicated are the two major rift systems that formed superimposed on the NCC: The Paleogene North China Basin (in green, modified from Qi and Yang, 2010) and the Neogene circum-Ordos Rifts (in red, modified from Zhang et al., 2003; Deng et al., 2007). Bold black lines indicate the major strike slip fault zones that effect present-day deformation.

The Shanxi Rift is part of a Cenozoic rift system which is known as the Circum-Ordos rifts, which surround the Western Block of the North China Craton (NCC) (Fig.1). Due to the strong lithosphere of the cratonic western block of the NCC, deformation was localised in two rift system along it: The Weihe-Shanxi Rift system in the southeast and the Yinchuan-Hetao rift system in the northwest (Zhang et al. 2003). Timing of these is debated with some authors arguing for Oligocene-Eocene initiation of the Weihe, Hetao and Yinchuan rifts with the Shanxi Rift being younger (Zhang et al. 2003; Shi et al. 2020) while other authors argue for a late Miocene initiation for all rifts (Yin, 2000). The Shanxi Rift in North China contains faults with a variety of trends which formed in the Late Miocene to present day (Su et al., 2023) (Fig.1). The origin of these trends is unclear but the currently accepted model postulates multiple changes in stress axes orientation during transtensional evolution of the Shanxi

Rift since the late Miocene, with strain being partitioned into dip-slip and strike-slip fault systems during transtension (Shi et al. 2015a). There has been little focus on the influence of structural inheritance on the wider evolution of North China, with a few exceptions that show active normal faults often follow the trends of inherited structures (Su et al. 2021) and possibly detach into low angle shear zones at depth (Pavlides et al. 1999). Major faults in the Shanxi Rift commonly expose basement massifs of the Trans North China Orogen (TNCO) in their footwalls. The TNCO formed during the collision of the Eastern and Western Block of the NCC in the Paleoproterozoic. While these basement massifs have been intensively studied to unravel the exact timing and kinematics of the Proterozoic collision (Kusky and Li, 2003; Zhao et al., 2005; Trap et al., 2007, Trap et al., 2008; Faure et al., 2007; Trap et al., 2009a; Trap et al., 2009b; Zhai et al., 2010; Zhai and Santosh, 2011), the role of these basement massifs on the late Cenozoic rifting in the Shanxi Rift has not been considered in detail.

There is limited seismic reflection data available for the Shanxi Rift (Xu et al., 1993; Ai et al., 2019). However, the degree of tectonic activity and subaerial exposure makes it possible to use geomorphology to study the structural evolution. In active rifts geomorphology and surface expression of faults is a commonly used to study the tectonic evolution of a rift, that has been successfully employed in regions such as the Basin and Range (Jackson and Leeder, 1994; Densmore et al., 2003; Densmore et al., 2004), the Apennines (Whittaker et al., 2008; Geurts et al., 2020; Fisher et al., 2022), the Gulf of Corinth (Leeder and Jackson, 1993; Goldsworthy and Jackson, 2000; Gallen et al., 2021) or the East African Rift (Erbello et al., 2022; Dulanya et al., 2022). These geomorphic approaches are varied and include studying the drainage evolution, the topographic response to faulting or using rivers to track the transient uplift rate. Landscapes are primarily formed by two competing forces: tectonics and erosion (Whittaker, 2012). Geomorphic indices have been used to quantify landscape response to tectonics (Bull and McFadden, 1980; Cox et al., 1994; Hamdouni et al., 2008; Gao et al., 2016; Markrai et al., 2022). This study uses three indices, hypsometric integral, channel steepness and local relief, to evaluate the landscape response to faulting in the Shanxi Rift.

By using geomorphic analysis to evaluate the tectonic evolution of the Shanxi Rift, highlighting areas of increased tectonic activity, and comparing these with inherited structures, we provide new insights on the influence of inheritance on the evolution of the Shanxi Rift. Specifically, our results question the need for rapid changes in the Neogene strain field orientation to explain the varying fault orientations and fault evolution in the Shanxi Rift. Instead, we show a novel, simpler model whereby inheritance under a constant strain field creates a segmented rift system and creates RIZs where strain and earthquake activity are focused. More generally, our work shows how geomorphic indicators can be used to identify the most active (and potentially hazardous) faults in an active extensional system.
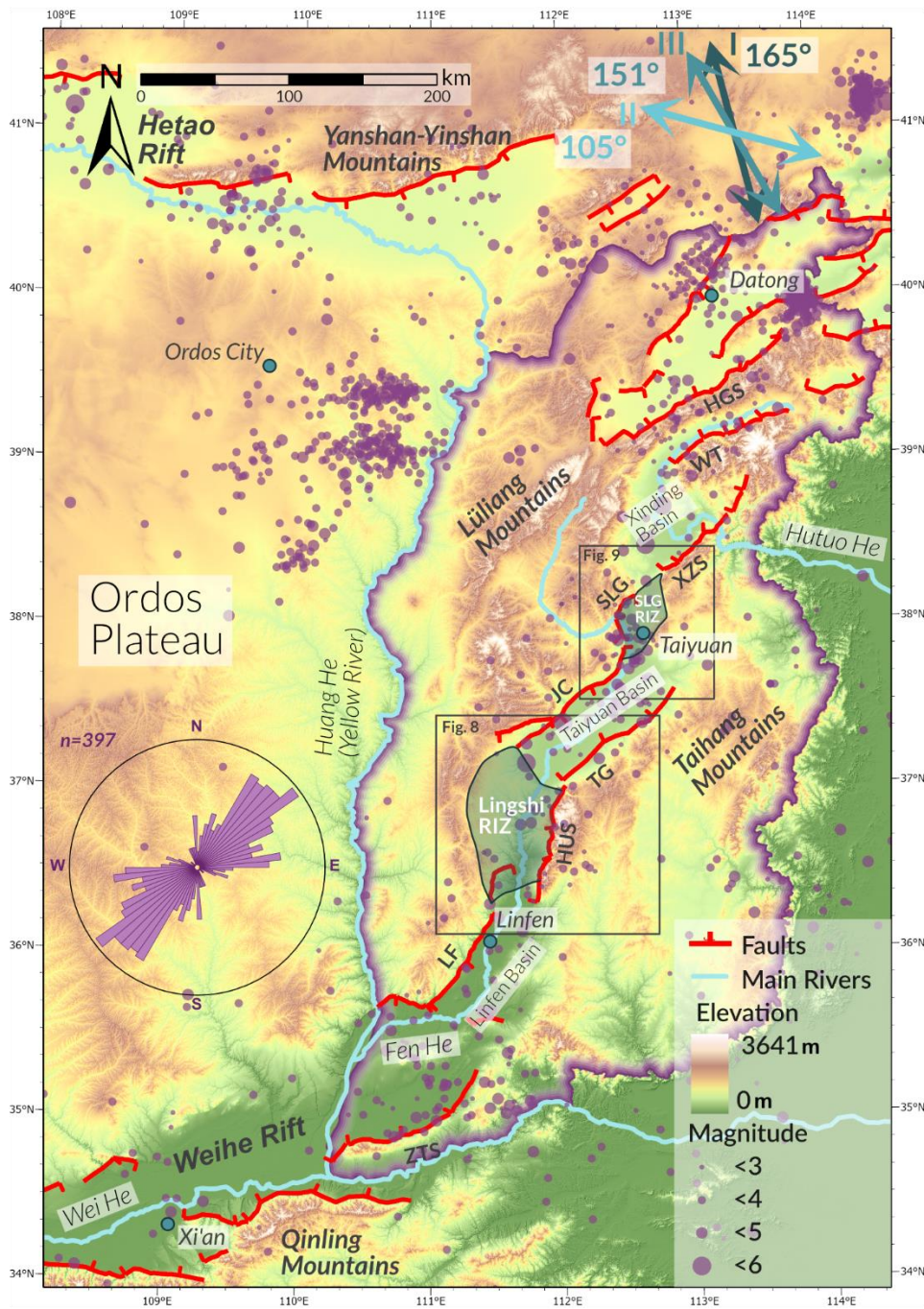
Figure 2: Detailed map of the circum-Ordos Rifts and the main rivers. Extension directions shown are from: I - Zhang et al. (1998) II - Shen et al. (2000) III - Middleton et al. (2017). Rose plot shows the mean orientation of major rift faults in the Shanxi Rift (defined here as the regions that lie within the purple bounding line). Faults were split into individual segments according to their orientation. Purple dots represent earthquakes from the ISC catalogue (Storchak et al., 2013; 2015; Di Giacomo et al., 2018) and are weighted

110

2 Geological Setting

The Shanxi Rift system in North China is an active continental rift system that is superimposed on the 1.8 Ga TNCO (Fig. 1)
115 when collision of the Eastern and Western Blocks formed the NCC. Exact timing and kinematics of this collision remain uncertain (Zhao et al., 2005; Kusky et al., 2007; Zhai and Santosh, 2011). Since the Proterozoic the NCC has been a stable cratonic block with a lithospheric thickness of 200 km, evidenced by Palaeozoic kimberlites (Menzies et al. 1993; Griffin et al., 1998; Menzies et al., 2007). The Paleoproterozoic and Archean basement rocks are unconformably overlain by the greenschist facies metasedimentary rocks (Faure et al. 2007) of the Paleoproterozoic Hutuo Group which was deposited in a
120 foreland basin during the TNCO orogeny (Li et al. 2010). The lower Palaeozoic cover consists of Cambrian continental siliclastic successions, followed by shallow marine carbonates and Ordovician platform carbonates. Carboniferous and Permian rocks were deposited in changing shallow marine to fluvio-deltaic conditions and contain coal measures. These are topped by Mesozoic continental clastics, grading into cross-bedded aeolian sequences in the Jurassic (SBGMR, 1989). This evolution led to a clear division of lithologies in the Shanxi Rift, the Paleoproterozoic rocks which include all the rocks that
125 made up the TNCO, including Archean Tonalite-trondhjemite-granodiorite complexes, high-grade metamorphic rocks such as greenstone belts and orthogneisses as well as post-orogenic granites. These rocks are referred to as Paleoproterozoic crystalline rocks in this study (dark brown in Fig.3) and are very resistant to erosion. The second group comprises the cover sequence of these rocks and is principally composed of low-grade metamorphic rocks such as clastic metasediments and carbonates of Mesozoic and Palaeozoic age, which are referred to as low-grade metasediments in this study (blues and greens in Fig.3).

130
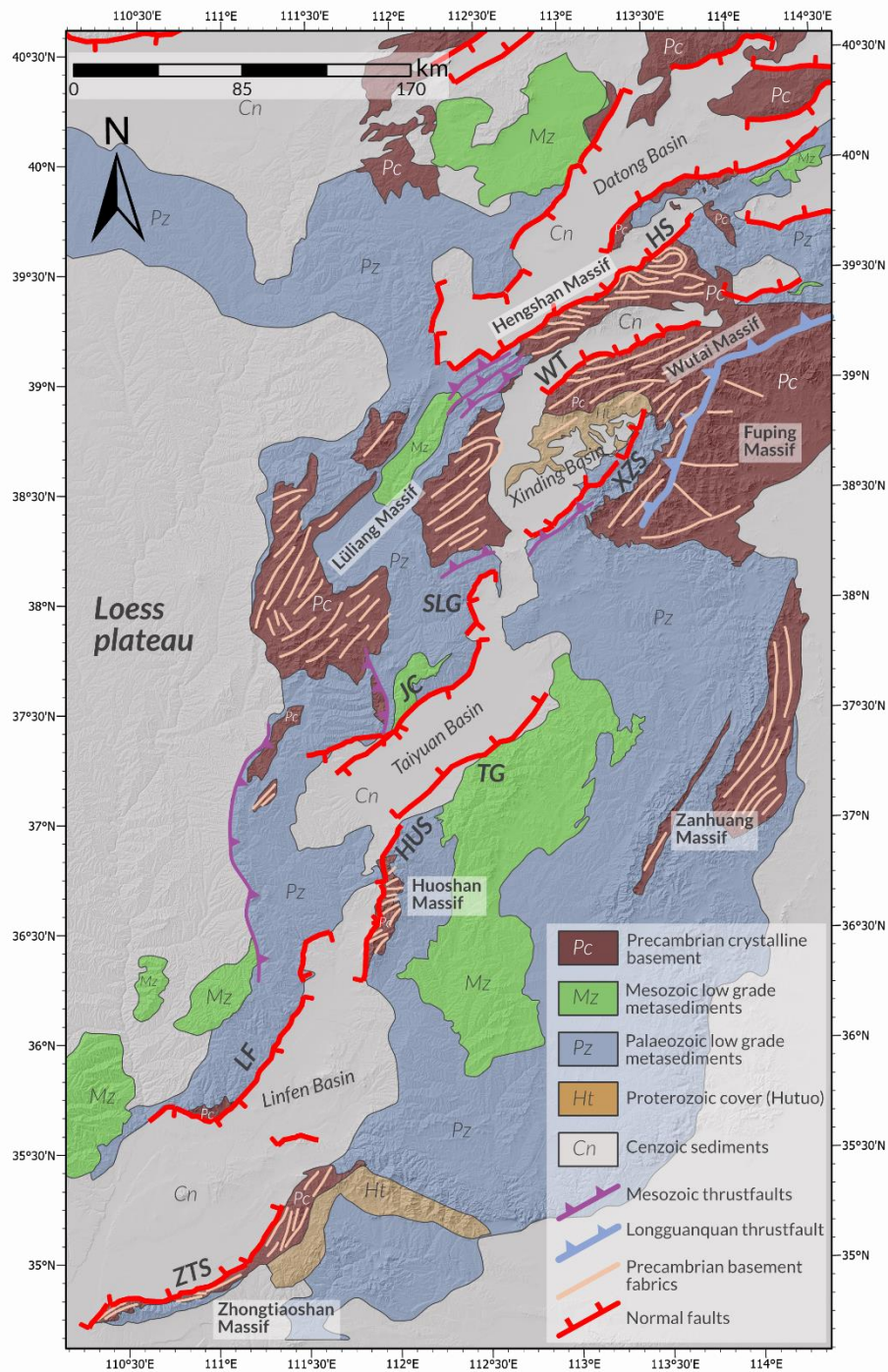
Figure 3: Simplified geological map of the Shanxi Rift (modified from SBGMR, 1989 and Clinkscales et al., 2021) showing the main pre-existing structures of the study area (Faure et al., 2007, Trap et al., 2007, Trap et al., 2009, Zhang et al., 2011; Clinkscales and Kapp, 2019). Main metamorphic fabrics are indicated in light brown lines which are predominantly orientated NE-SW.

Since the Mesozoic, parts of the NCC have been destroyed by thermal erosion (Griffin et al., 1998; Menzies and Xu, 1998) and/or partial delamination (Gao et al., 2002; Gao et al., 2004) which is likely to be connected to the subduction of the palaeo-Pacific underneath East Asia (Menzies et al., 2007; Zhu et al., 2012). The Eastern and Western part of the NCC underwent a different evolution during the Mesozoic. The Eastern part experienced compressive deformation during the Jurassic to Early Cretaceous (Davis et al., 2001) also regionally known as the Yanshanian Movement (Wong, 1927, Dong et al., 2015) which was less pronounced within the Western Block. However, Paleoproterozoic orogenic belts like the TNCO also record this widespread compressional event (Zhang et al., 2008; Zhang et al., 2011; Clinkscales and Kapp, 2019). Since the Early Cretaceous the eastern NCC experienced extension, resulting in structures such as pull-apart basins, core complexes and associated voluminous magmatism (Zhu et al., 2012). Destruction of the cratonic lithosphere was limited to the Eastern NCC, which resulted in Mesozoic magmatism almost exclusively affecting the Eastern NCC (Zhu et al. 2012). Here, the North China Basin formed in the Eocene-Oligocene (Allen et al., 1997). This basin has transtensional kinematics, which give it a resemblance to a giant pull-apart (Chen and Nabelek, 1988; Farangitakis et al., 2020). During the Paleogene, the Western NCC experienced limited extension. The Shanxi Rift is one of a series of Neogene, narrow rifts which follow the trend of Precambrian orogenic belts within the NCC, developing around the Ordos Block (Shi et al., 2020).

The Shanxi Rift is a NE-SW trending rift system that consists of a series of left-stepping en-echelon basins. (Zhang et al., 2003) (Fig. 2a). The system is ~1000 km long and ~300 km wide and is bound to the north by the Yinshan-Yanshan Range and to the south by the Qinling Range. It is commonly believed to have initiated in the Late Miocene based on the oldest sediments found in the rift grabens - the Kouzhai Formation (Xu et al., 1993). The crust beneath the Shanxi Rift is ~32-39 km thick and is thinner in the basinal regions than adjacent to the Lüliang and Taihangshan highlands, which flank the rift to the west and east (Chen, 1987, Tang et al., 2010). The Shanxi Rift is characterized by a series of distinct rift basins that have either half graben or graben geometries, separated by two topographically higher elevated areas which have previously been called push-up swells but are referred to here as RIZs (Fig. 2) (Xu and Ma, 1992; Xu et al., 1993). The Linfen Basin to the south is separated by the Lingshi RIZ from the Taiyuan Basin, which is in turn separated from the Xinding Basin in the North by the Shilingguan RIZ. There are two main rivers that drain the Linfen-Taiyuan-Xinding basin system of the Shanxi Rift: The Hutuo River draining towards the East across the Xizhoushan Fault into the North China plain while the Fen River is diverted to the South where it drains into the Yellow River (Fig. 2), with the main drainage divide between these represented by the Shilingguan RIZ. The synrift thickness across the Shanxi Rift varies; While the Taiyuan basins has the thickest synrift sediment thickness of up to 3800m (Xu et al. 1993), the Xinding only contains up to a 1800m (Xu et al. 1993) and the Linfen basin contains up to 2200m of synrift fill (Su et al., 2023). The Shanxi Rift shows a widespread seismicity of M_w 3-5 events on USGS and ISC records (Fig.2), but the rift has produced infrequent but devastating earthquakes in historical time. The AD 1303 Hongdong Earthquake is believed to have been an M_W ~7.5 event (Xu et al., 2018) and is well-documented in Chinese

historical writings. Shanxi Province itself is densely populated with 36.5 million inhabitants. Large cities like Taiyuan (5 million inhabitants), Linfen (4 million inhabitants) and Datong (3 million inhabitants) are close to active faults.

Constraining the exact extension direction and rate is difficult due to the Shanxi Rift's low extensional strain rate. A variety of researchers have used field-based fault slip measurements, GPS derived velocities and/or earthquake focal mechanisms to constrain the extension direction. Studies by Shen et al. (2000), He et al. (2003) and Middleton et al. (2017) constrain the extension direction in the Shanxi Rift to between 105° and 165° and extension rate as being between 0 and 6mm/year (Fig. 2). Other studies using field-based measurements (Shi et al., 2015a; Assie et al., 2022) propose a complex evolving strain field that has changed throughout the Cenozoic. According to these studies, NW-SE extension in the Mio-Pliocene initiated the rifting in Shanxi and was followed by NE-SW extension in the early Quaternary leading to further subsidence. Theses authors suggest that the current NNW-SSE extension strain field developed at 0.11 Ma and marked a shift from NW-SE extension to right lateral deformation in the Shanxi Rift, dated using faulted basalts of that age in the Datong Basin (Shi et al., 2015a). Shi et al. (2015b) and Shi et al. (2015a) relate these changes in the strain field to growth of the Tibetan Plateau.

3 Methods

3.1 Pre-Rift Architecture and Structural Mapping

We compiled a map of the structures in the Shanxi Rift (Fig. 3) by digitising basement fabrics, thrust faults, shear zones and active faults from published maps in ArcGIS Pro™. Additionally, we compiled published structural data from the Paleoproterozoic basement complexes to plot on stereonets. In this study we primarily focus on the influence of inherited structures in the Palaeoproterozoic basement on the evolution of the Shanxi Rift, therefore if not specified otherwise we refer to Palaeoproterozoic structures when discussing basement or inherited fabrics. To map the active fault structures, we identified linear breaks in the landscape on SRTM topographic data with 90 m resolution (https://lpdaac.usgs.gov/products/srtmgl3v003/) aided by slope and curvature attributes. This resolution is appropriate for the larger regional scale of this study and helped keep computing power demands manageable. We define active faults as linear, steep scarps (>20-30°) that offset Quaternary sediments, similar to the approach by Wedmore et al. (2022). Furthermore, we used topographic profiles across faults and geomorphological features such as steepened river channels and triangular facets along the fault scarp as features guiding our identification of active normal faults. Figure 2 shows a topographic map and location map of the study area.

3.2 Geomorphic Indices

We used geomorphic indices to quantify the landscape response of the Shanxi Rift to tectonic drivers. We analysed the morphometric indices from 10873 1st order drainage basins located in the Shanxi Rift, extracted from the SRTM dataset using Topotoolbox2 Matlab scripts (Schwanghart and Scherler, 2014). We focused in this study on three geomorphic indices, 1) local relief, 2) the Hypsometric Integral (HI) and, 3) the normalised channel steepness (k_{sn}) as these proved to be the most helpful and discerning when evaluating the tectonic signals (Pérez-Peña et al., 2009; Gao et al., 2016; Obaid and Allen, 2019;

Groves et al., 2020; Erbello et al., 2022). Using R, we also generated violin plots that visualise the distribution of values for each geomorphic index. The shape of the "violins" represents the distribution of values as the violin will be thicker the more data points sit at that range. Using these violin plots we can also assess the impact of lithology on the geomorphic indices to enable us to compare the distribution of values per fault to the dominant footwall geology of the fault and assess if lithology is the principal factor determining the distribution.

3.2.1 Local Relief (R_l)

Local relief is a commonly used measurement of the variation of topography over an area to analyse spatiotemporal tectonic trends (Ahnert, 1970; Schmidt and Montgomery, 1995; DiBiase et al., 2010). The relief R_l was calculated as the maximum difference in elevation E over; 1) a delineated drainage basin (S1) or 2) within a circular moving window with a 1 km radius:

$$R_l = E_{max} - E_{min} \hspace{6cm} 1)$$

where R_l is the local relief and E refers to elevation. High relief landscapes therefore show a higher variation of elevation over an area, which may indicate faster uplift rates. However, local relief is also influenced by lithology, high relief landscapes can also be the result of resistant lithologies with low erodibility (Ahnert, 1970).

3.2.2 Hypsometric Integral (HI)

The Hypsometric Integral (HI) was first used as a geomorphic index by Strahler (1952, 1957). It is a measurement of the distribution of elevation within an area. HI is derived as the integral of the hypsometric curve, which plots normalised elevation over normalised drainage area for each drainage basin. Fig.4 illustrates the theory behind HI. The interpretation of the hypsometric curve assumes that topographically more youthful basins will have a convex-up shaped curve while more mature ones will have a more concave-up shape. If uplift outpaces erosion, there will be a greater range of elevation over an area which results in a convex-up shaped curve and a high HI. Therefore, high HI values should coincide with rapidly uplifting areas (e.g., footwalls of active normal faults) (Hamdouni et al., 2008; Perez-Pena et al., 2009; Obaid and Allen, 2019; Groves et al., 2020; Erbello et al., 2022). HI may be influenced by other factors than tectonic uplift such as climate, lithology and basin shape and area. Lifton and Chase (1992) propose that at larger scale analysis (>1000km) tectonics will play have a larger effect than lithology, while at smaller scales lithology can have a considerable impact. Masek et al. (1994) proposed that climate can influence the hypsometry of an area. Several studies proposed that basin shape and area influence the HI of a basin (Lifton and Chase, 1992; Masek et al. 1994; Hurtrez et al., 1999; Chen et al., 2003), however Walcott and Summerfield (2008) analysed the basins of southern Africa and could find no impact of basin scale on HI. High HI regions may often be indicative of fast uplift rates but could also be related to other factors therefore when analysing the tectonic implications of HI it is important to be aware of these limitations. To mitigate the effect of lithology on our tectonic analysis we also compare the HI distribution per fault with the predominant lithology of the fault's footwall using violin plots generated with R.
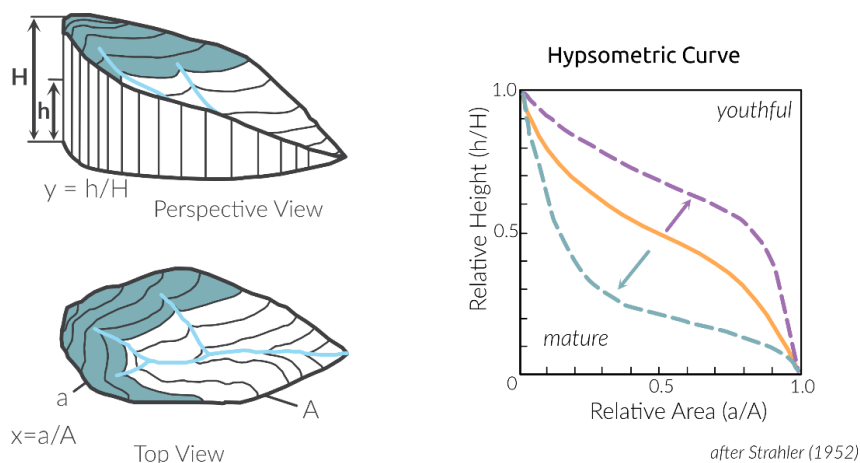
Figure 4: Schematic diagram explaining the concept of the Hypsometric Integral (after Strahler, 1952). Every drainage basin is dissected into elevation bands to determine a ratio of relative height over relative area. Concave curves indicate more youthful topography while convex shaped ones indicate more mature topography.

In this study we calculated the HI per drainage basin (Obaid and Allen, 2019; Groves et al., 2020). The shape and size of drainage basins is controlled by tectonic and geological features, therefore they are more natural boundaries for comparing areas of variable uplift and erosion rates than calculating HI with an arbitrary moving window. We calculated the hypsometric curves using QGIS 3.16 and derived the integral for each curve through an R script (Supplementary material X1).

3.2.3 Normalised Channel Steepness (k_{sn})

Normalised channel steepness (k_{sn}) is a frequently used topographic metric in tectonic geomorphology (DiBiase et al., 2010; Whittaker and Walker, 2015). For steady-state landscapes, meaning rock uplift rates and river incision rates are at equilibrium, the channel slope S is defined as a power law function (Hack, 1957; Flint, 1974):

$$S = k_s A^{-\theta} \tag{2}$$

where A is the drainage area. The parameter k_s is the channel steepness index, and θ denotes the channel concavity index. (Snyder et al. 2000). In natural landscapes, its well known that variations in the best-fit for concavity index (θ) has a significant impact on estimates of k_s. To circumnavigate the problem, we used a reference concavity index of 0.45 (Wobus et al. 2006). Using this reference concavity index results in a dimensionless "normalised" channel steepness k_{sn}. Variations in k_{sn} along channel segments may be related to changes of the uplift rate of that region (Snyder et al., 2000; Whipple, 2004) with higher k_{sn} values often indicating higher uplift rates.

We used the TopoToolbox2 Matlab scripts (Schwanghart and Scherler, 2014) to extract the river profiles and calculate the normalised channel steepness from smoothed river profiles. This approach is built upon the method developed by Perron and Royden (2013) to analyse river profiles. We extracted streams with a drainage area of above 1 km^2 to avoid hillslope areas.

250 Normalised channel steepness (k_{sn}) is commonly applied to stream networks to visualise knickpoints (variations in the slope of river channels) in rivers. In this study we used Topotoolbox2 to calculate the basin averaged k_{sn} values. This is achieved by calculating the mean of all k_{sn} values in each drainage basins. This makes it easier to compare the k_{sn} values to those for local relief and HI. The k_{sn} stream network map is available in the supplementary material (S2).

Shanxi Rift Fault characteristics							
Fault	Trend (in degrees)	Footwall lithology	Mean R_l	Mean HI	Mean k_{sn}	Geomorphic response	Orientation of inherited structures
Hengshan	57	Crystalline Basement	234	0.33	68	medium	ENE-WSW
Wutai	65	Crystalline Basement	367	0.37	79	high	NNE-SSW
Xizhoushan	50	Crystalline Basement	320	0.36	72	high	NE-SW
Shilingguan	5	Low-grade metasediments	217	0.4	57	high	NE-SW
Jiaocheng	48	Low-grade metasediments	193	0.32	39	low	NE-SW
Taigu	49	Low-grade metasediments	168	0.29	33	low	NE-SW
Huoshan	12	Crystalline Basement	301	0.36	68	high	NE-SW
Linfen	38	Low-grade metasediments + Crystalline basement	219	0.38	47	medium	E-W
Zhongtiaoshan	72	Crystalline Basement	208	0.31	43	medium	NNE-SSW

255 **Table 1: Summarising the Fault and their geomorphological response as well as their lithology and the orientation of the inherited fabrics in vicinity of the fault.**

4 Results

4.1 Pre-rift structural architecture

The northern part of the Shanxi Rift is dominated by uplifted Paleoproterozoic basement massifs. The Hengshan, Lüliang,
260 Wutai and Fuping massifs are exposed in the footwalls of major basin bounding faults (Fig. 3, 5). In the south the footwalls are more commonly dominated by Mesozoic and Palaeozoic sedimentary rocks with notable exceptions being the Huoshan and Zhongtiaoshan faults, which also expose Paleoproterozoic metamorphic basement at surface.

The general trend of most Paleoproterozoic structures is broadly NE-SW, which is sub-parallel to the active rift faults. In the
265 northern basement massifs (Hengshan and Wutai) there is a subtle change to WNW-ESE-trends (Fig. 3, 5). The dip of these structures is variable due to folded nature of these rocks (Trap et al., 2007; Trap et al., 2009a; Clinkscales and Kapp, 2019). The dip of the fabric's changes from dipping towards and away from the faults along strike and the dip of the fabrics ranges from 25-85° (Trap et al., 2007; Trap et al., 2009a) The orientations also show plunging fold geometries in the basement massifs of the Hengshan and the Lüliangshan mountains (Stereonets Hengshan and Lüliang, Fig.5). The Fuping Massif displays a
270 considerable spread of basement fabric trends that can be split into two groups: fabrics trending NE-SW in the NW and fabrics

with an NNW-SSE trend in the SE (Stereonets Fuping-West and Fuping-East, Fig.5). These two regions are separated by the NE-SW trending Longguangquan thrust fault (marked as a blue thrust fault on Fig. 3 and 5) which most likely originated as a shallow-dipping thrust fault in the Paleoproterozoic (Trap et al., 2008). The basement fabrics in the NW-part and the Longguangquan thrust fault are parallel to the Xizhoushan Fault. Further north the Paleoproterozoic basement fabrics of the Wutai complex are orientated ENE-WSW which is mirrored by the active normal Wutai Fault.
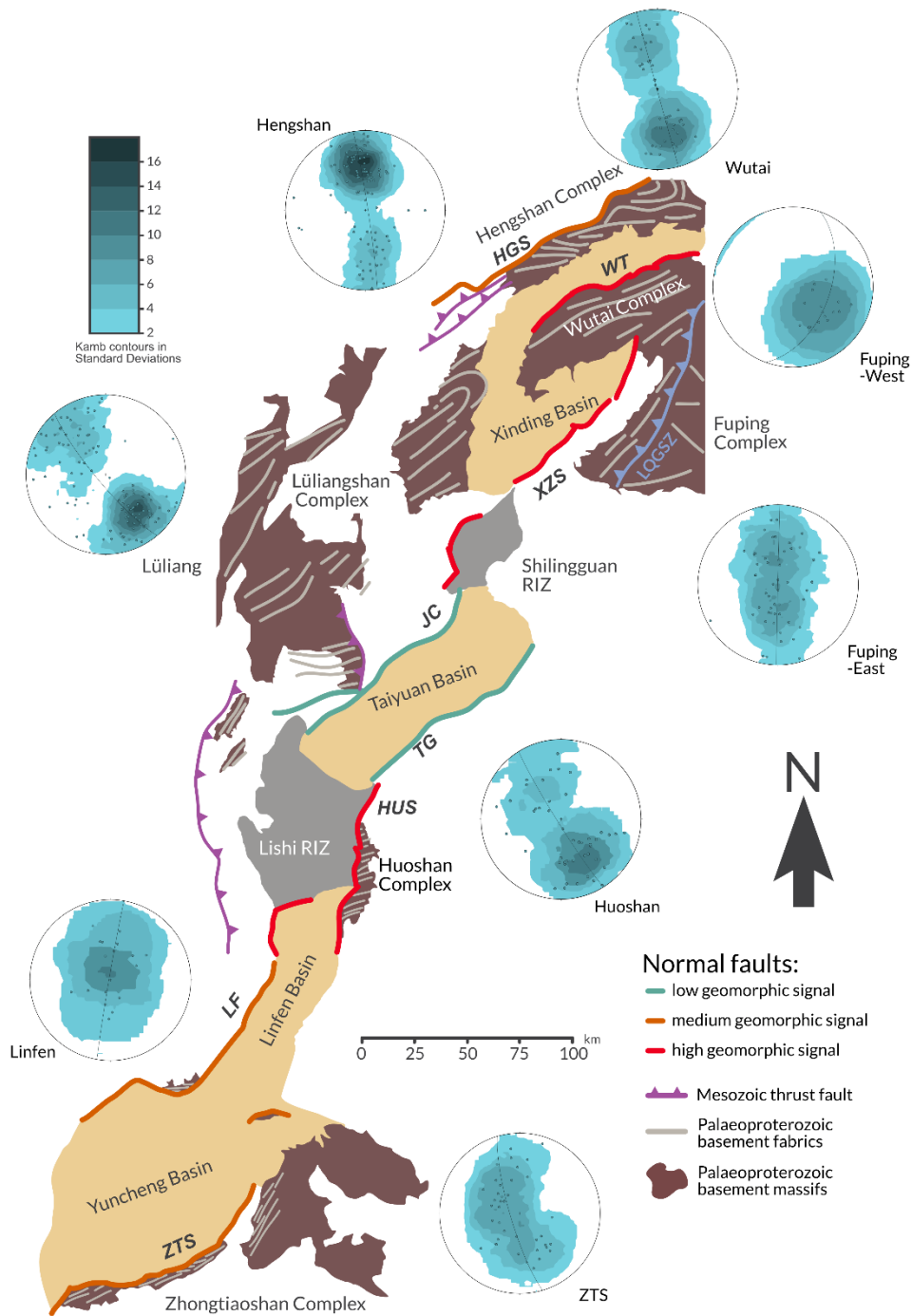
Figure 5: Schematic fault map of the Shanxi Rift with faults colour coded according to their geomorphic signal – compare with Table 1. Exposed basement of the TNCO in brown with the main structural trends highlighted in light grey. Stereonets of poles to

280 planes (data from Trap et al., 2007; Trap et al., 2009a) show the structural grain of the main basement complexes. Most basement complexes show a NE-SW orientated grain, but it is more ENE-WSW in the north of the Shanxi Rift (Wutai/Hengshan).

285
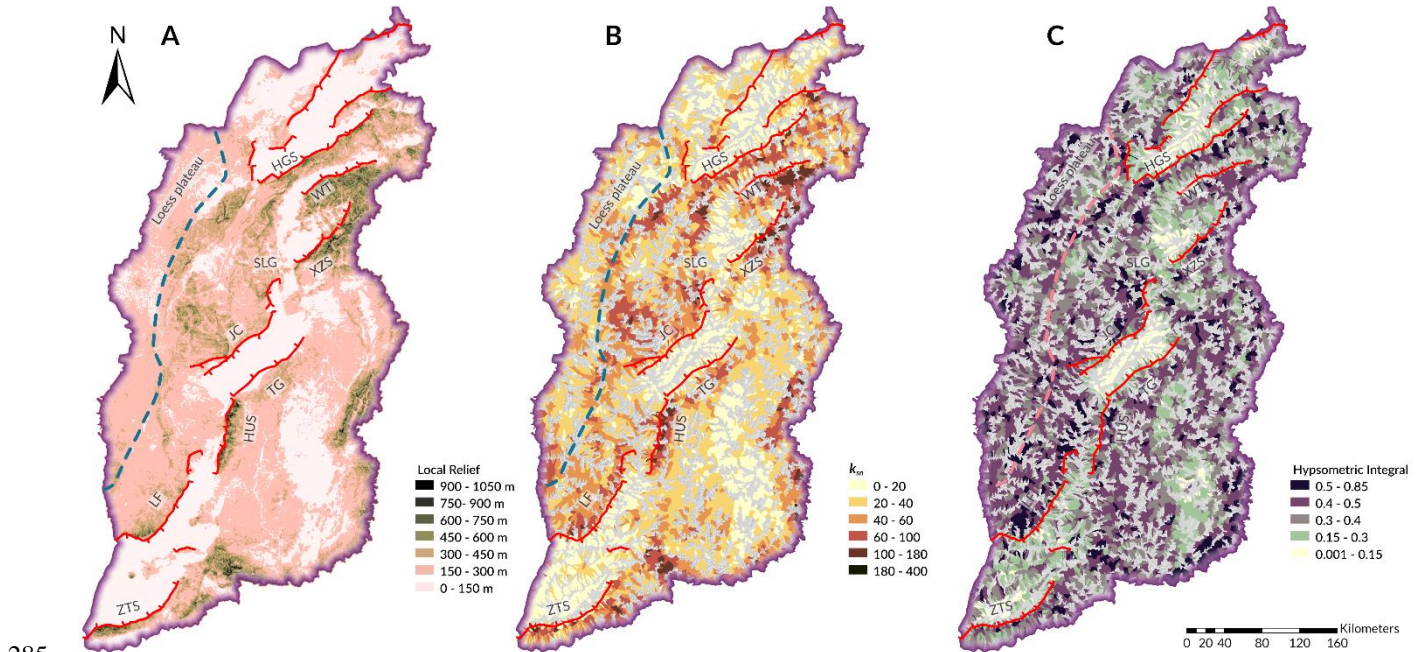
Figure 6: Geomorphic indices map of the Shanxi Rift. Major extensional faults shown in red, boundary of the Loess plateau indicated by dashed line A) Local relief map. Darker colours indicate higher relief regions. Local relief was calculated within a 1km circular radius. High relief is found especially in the northern Shanxi Rift in the footwalls of the Wutai and Xizhoushan faults as well as further south along the Huoshan and Zhongtiaoshan faults. Noticeably lower local relief values occur along the central Jiaocheng
290 **and Taigu faults. B) Mean normalised channel steepness (k_{sn}) calculated for 1st Strahler order basins. High values are commonly located in the footwalls of active faults, especially the Wutai, Xizhoushan and Huoshan faults. Low values are found in the lower lying basin regions. Central faults (Taigu and Jiaocheng) show noticeably less high k_{sn} basins than other faults. C) Hypsometric Integral (HI) calculated for 1st Strahler order basins. High values are commonly located in the footwalls of active faults, especially the Wutai, Linfen, Shilingguan and Huoshan faults. Low values are found in the lower lying basin regions.**

295 **(Abbreviations: HGS-Hengshan; WT-Wutai; XZS-Xizhoushan; SLG-Shilingguan; JC-Jiaocheng; TG-Taigu; HUS-Huoshan; LF-Linfen; ZTS-Zhongtiaoshan)**

4.2 Local Relief (R_l)

The local relief of the region (Fig. 6a) closely follows the overall topography of the region but emphasises certain features to make them easier to identify. Two areas of high local relief can be identified in the north and south of the Shanxi Rift.

300 In the northern region around the Wutai and the Xizhoushan faults, the footwalls of the prominent bounding faults are highly elevated (2500-3000 m) and show local relief values exceeding 1000 m. In the southern part of the Shanxi Rift, the Huoshan Fault to the south also shows high local relief (>1000 m) in the footwall close to the bounding fault. These high relief faults in

Shanxi show consistently high local relief values along their fault traces whereas the Zhongtiaoshan Fault has high local relief (>1000 m) along the western end of the fault but lower values towards the east.

305   The Shilingguan RIZ is characterised by shorter faults segments, and this region shows an elevated local relief of around 500 m. In some examples, in footwalls close to the main fault, the local relief exceeds 1000 m. This is seen where a broadly N-S trending fault and a broadly NE-SW trending fault intersect and link up. Further into the footwall of this fault, there are pockets of high (>1000 m) local relief, which are along the sides of the narrow gorge of the Fen River. Compared to faults in the North and South of the Shanxi Rift such as Huoshan, Zhongtiaoshan or Wutai Fault, the elevation in this area is lower (~1500 m) but

310   the local relief remains comparatively high (up to 1000 m). The two longest faults in the central region of the Shanxi Rift, bound the Taiyuan Basin (Taigu and Jiaocheng), show a lower local relief response rarely exceeding 450 m, with elevation lying between 1500 and 2000 m. There are regions of medium-high values of local relief (450-750 m) away from active structures, for example in the Taihangshan mountains or to the west of the Lingshi RIZ.

315   The per fault distribution of relief values (Fig. 7a) shows a clear divide between faults. The faults which have Proterozoic basement rocks in the footwall (Huoshan, Xizhoushan, Zhongtiaoshan, Hengshan and Wutai) have a greater range of values often exceeding 400 m. This is especially pronounced for the Wutai and Xizhoushan faults. The Hengshan fault is slightly different as its distribution of relief values is closer to the faults with Palaeozoic-Mesozoic sedimentary rocks in the footwall having most of its values between 200-300m. The Zhongtiaoshan has a maximum at around 200m and therefore lower relief than the other faults but still has some values in the higher ranges with max values of 600m. The faults with Palaeozoic and

320   Mesozoic sedimentary rocks in the footwall (Shilingguan, Taigu, Jiaocheng and Linfen) have overall lower values and a smaller range of values. Most of their values lie between 200-300 m but their minimum values are below 100m. Shilingguan as the RIZ fault shows a similar maximum at 200-300m but is missing the low minimum values resulting in a more compact distribution.

325   **4.3 Normalised channel steepness (k_{sn})**

Four regions show high basin averaged k_{sn} values (Fig. 6b): The Huoshan Fault, the Xizhoushan Fault (especially its northeastern part), the Wutai Fault and the Zhongtiaoshan Fault. These are the same regions that show high local relief (Fig. 6a and Section 4.2). Low values of less than 50 are rarely associated with obvious faults with a surface trace. The Jiaocheng and the Taigu faults footwalls have drainage basins with k_{sn} values between 50-85 which reflects the local relief response of

330   these faults (Fig. 6a). The footwall of the fault bounding the Shilingguan RIZ shows elevated values. Notably the area where the broadly N-S and NE-SW trending faults link up show basins with k_{sn} exceeding 100. The k_{sn} value distribution (Fig. 7b) of the different faults shows a similar trend to the Relief as there is a good separation between faults with different basement lithology. The faults with Proterozoic basement show much higher values reaching values of 200 while the faults with Palaeozoic-Mesozoic basement show narrower distributions rarely exceeding 100 and most values lying below 50. The notable

335   outliers here are Hengshan whose distribution again is more similar to the Palaeozoic-Mesozoic basement faults. Here the

Shilingguan RIZ records much higher values than the other faults with Palaeozoic-Mesozoic basement footwalls and has a distribution more similar to the Proterozoic faults.

4.4 HI

While the local relief and the channel steepness showed broadly similar distributions, the HI differs slightly and shows a more
340 distributed pattern of high (>0.5) HI basins (Fig. 6c). The footwall blocks to the Wutai, Xizhoushan and Zhongtiaoshan faults show elevated responses but in contrast to the previously described geomorphic parameters they do not show the highest values. In the footwalls of these faults, HI values mostly range between 0.3-0.5 and only isolated regions go above 0.5. The bounding fault of the Shilingguan RIZ has among the highest HI responses with values often exceeding 0.5 and rarely below 0.4. The Lingshi RIZ that is bounded by the Huoshan Fault also shows elevated values compared to the surrounding basins,
345 due to its overall higher elevation and dissected topography. These high HI values match spatially with the high local relief and k_{sn} values. Therefore, the Shilingguan RIZ and Huoshan Fault have consistently higher values compared to the Wutai, Zhongtiaoshan or Xizhoushan footwalls. The Linfen fault adjacent to the Lingshi RIZ also shows elevated HI basins (>0.5), especially towards the southern end where it shows a distinct fault bend, however these high HI values are not matched to the same degree by local relief and k_{sn} (Section 4.2/3). The Taigu fault has lower HI values (below 0.4), matching the low values
350 for channel steepness and local relief. While the Jiaocheng fault has a greater spread with low values basins (0.2 – 0.4) but also higher HI value basins (0.5 – 0.85), especially towards the northeast of the fault as it approaches the Shilingguan RIZ.

High value HI basins (>0.5) are also found in regions away from the active normal faults that showed no recent tectonic activity. High values are observed to the west of the Shanxi Rift in the Loess Plateau on the western edge of the HI map. (Fig.
355 6c) Similar to the relief and the channel steepness, high values are also observed in high elevation regions further away from mapped active faults. These commonly correspond to known thrust faults or other contractional structures (SBRGM, 1989) which were last active in the Mesozoic and created relict topography.

The HI value distribution (Fig. 7c) differs from the previous two geomorphic indices significantly as a clear separation based
360 on lithology/footwall age is not obvious anymore and the patterns are more dispersed. The general trend still appears that faults with Proterozoic basements have slightly higher values (~0.5), however the Zhongtiaoshan fault while reaching very high HI values has most values sitting at 0.4 which is below the other faults with Proterozoic footwalls and closer to faults with Palaeozoic-Mesozoic sedimentary rocks in the footwall. Within these faults the Linfen and Shilingguan fault show higher values than the other two faults (Taigu and Jiaocheng). Overall, the Shilingguan and Huoshan faults within the RIZs record
365 the highest values but they are not significantly elevated over for example: Wutai or Linfen.
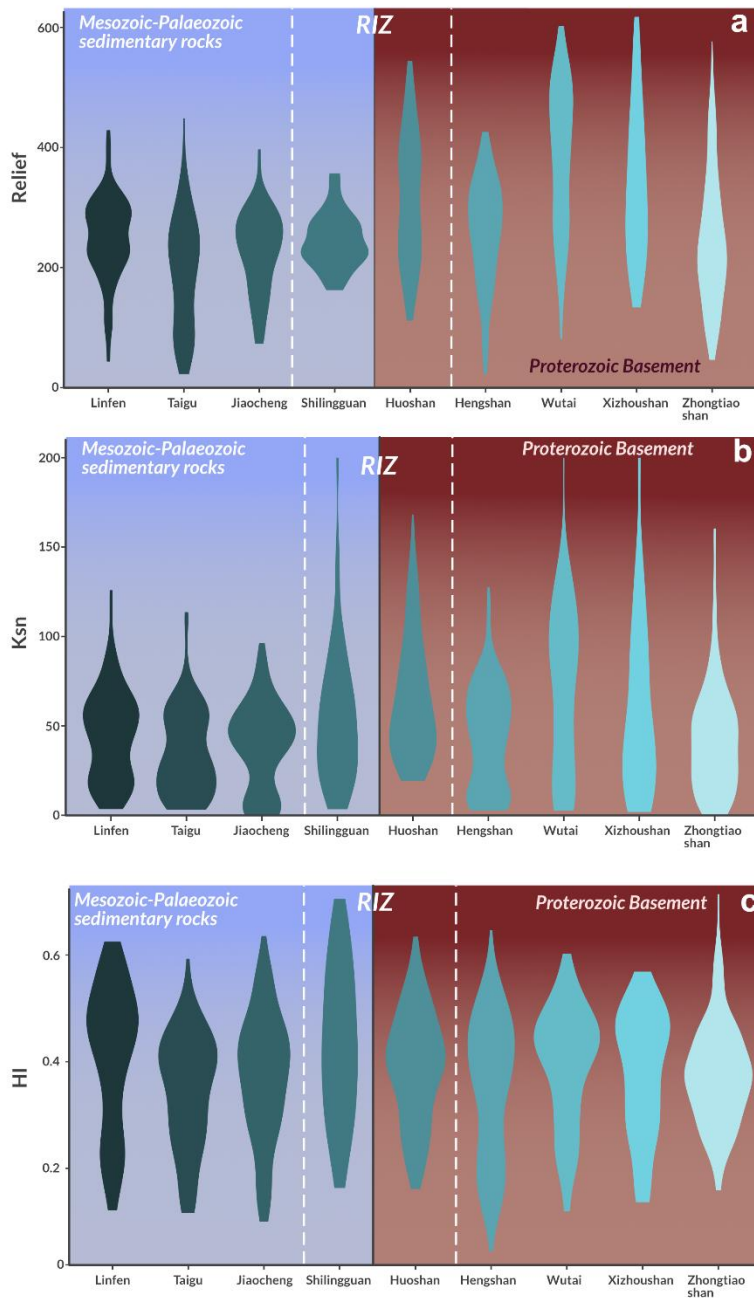
Figure 7: Violin plots showing the distribution of geomorphic values for each fault. Background shows the dominant footwall composition of the faults with RIZ faults plotted in the middle. A) Relief. Clear separation of faults with high values all having Proterozoic basement-dominated footwalls. B) k_{sn} values showing a similar separation to the mean relief. C) HI values show more distributed values. RIZ tend to have high geomorphic values (see main text for more discussion on this)

5 Discussion

5.1 Lithology dependence of geomorphic indices

375 The distribution of geomorphic indices for each fault shows significant differences (Fig. 7). Geomorphic response may be influenced by climate, lithology, and tectonics. The climate across Shanxi is continental and shows broadly little variation in precipitation (supplementary material S3; Fick and Hijmans, 2017) across the study region, which makes the differences in geomorphology between faults unlikely to be controlled by the climate. The lithology in Shanxi is more variable, as seen in Figure 3. The various lithologies can be divided into two main groups that differ in rock strength and erodibility. There are

380 Precambrian crystalline rocks which include Archean Tonalite–trondhjemite–granodiorite complexes, high-grade metamorphic rocks and post-orogenic granites which are all part of the TNCO (Trap et al. 2012) and the low-grade metasediments units which include low grade clastic metasediments and carbonates from the Palaeozoic-Mesozoic (SBRGM, 1989). Here, we evaluate how these differences in lithology may have impacted the geomorphic response.

385 Local relief and k_{sn} (Figs. 6a, b) show the highest values where crystalline basement lithologies are exposed in the fault footwall. Faults with high mean local relief values (>300m) have "strong" crystalline basement in their footwalls (Huoshan, Wutai, Zhongtiaoshan) or are directly adjacent to these (Xizhoushan), while low values (~<200 m) are found in the faults with Palaeozoic-Mesozoic rocks in their footwalls. HI (Fig. 6c) does not show the same bimodal distribution between faults with different footwall lithologies. The highest HI values correspond to faults with both Proterozoic basement footwall rocks

390 (Huoshan, Wutai, Xizhoushan) and Palaeozoic-Mesozoic footwall rocks (Shilingguan, Linfen). Meanwhile low HI values are also found for footwalls of both lithologies (Hengshan, Taigu and Jiaocheng, Zhongtiaoshan). We can infer that the differences in HI values between these fault blocks is not likely to be caused by lithology but rather their tectonic history. This suggests that HI may be a more robust geomorphic index for analysing tectonic activity than relief or k_{sn} because it is less influenced by lithology. Our finding that HI is not primarily influenced by lithology agrees with previous studies (Obaid and Allen, 2019;

395 Groves et al. 2020). High HI values are often correlated with high uplift rates, especially in regions with variable uplift rates, higher HI values are found in regions of higher uplift (Hurtrez et al. 1999). Therefore, the high HI values found in the footwalls of the Huoshan, Wutai, Xizhoushan and Shilingguan fault indicate that these footwalls have been uplifted the most rapidly.

To the western edge of the Shanxi Rift is a region of medium-high HI basins that to do not correlate with mapped active faults.

400 This is likely due to the landscape that typifies the Loess Plateau west of the Shanxi Rift. Loess is unconsolidated wind-blown sediment that is prone to dramatic erosion that creates deep gullies and ridges which can lead to high HI values. The Loess Plateau formed in the Pleistocene and its linear ridges and gullies have been carved out by aeolian and fluvial forces (Kapp et al. 2015), therefore the high response of the Loess Plateau are related to young landscapes sculpted by surface processes rather than tectonic forces. This does not detract from the main statement that HI is less influenced by lithology, as loess is an extreme

405 case of unconsolidated sediment as opposed to the main groups of low-grade metasediments and Palaeoproterozoic crystalline

rocks. However, it does highlight that HI is sensitive to the presence of Loess, therefore when evaluating the tectonic response of an area this needs to be accounted for.

The dependence of some geomorphic indices on lithology is observed in many other areas around the world and highlights the importance of considering the local geology before interpreting the relevance of geomorphic indices (Wobus et al. 2006; Kirby and Whipple, 2012). However, by comparing different faults with similar basement geology the lithological impact can be reduced as theoretically they should have a similar rock strength and erodibility. This enables us to compare the landscape response of these footwall uplifts to tectonics. In the Shanxi Rift for example, the Huoshan fault on average has higher values for geomorphic indices than other faults with Paleoproterozoic crystalline rocks in the footwall. Comparing the response of faults with footwall exposures of low-grade metasediments rocks it becomes evident that the main bounding fault of the Shilingguan fault has a higher geomorphic response than the Jiaocheng, Linfen and Taigu faults. Here the difference in geomorphic response between the Shilingguan fault and the other faults with low-grade metasediments in their footwalls is even more pronounced than comparing faults with Paleoproterozoic crystalline rocks in the footwall where the difference between the Huoshan fault and for example the Hengshan or Wutai faults is less stark. It must also be noted that the Shilingguan fault shows a higher HI and k_{sn} value than faults with "stronger" Paleoproterozoic crystalline rocks in their footwalls (Hengshan, Zhongtiaoshan). By comparing faults with similar footwall lithology, we can show that the difference in geomorphic response is not solely down to lithology and most likely has a tectonic origin.

5.2 Implications for rift evolution, linkage and seismic hazard

Two significant zones in the evolution of the Shanxi Rift are the two RIZs: Shilingguan and Lingshi that form between the major basins. Both zones are generally more elevated than the surrounding basins, making them potential sediment sources (Gawthorpe and Leeder, 2000), which is also shown by their patchy thin sediment fill compared to the major basins (Xu and Ma, 1992), RIZs are classified on their geometrical organisation (rift segment faults are underlapping or overlapping, parallel, oblique or orthogonal). The two RIZs differ in this geometrical organisation, the Shilingguan RIZ can be described as underlapping parallel divergent RIZ while the Lingshi RIZ is an underlapping oblique convergent RIZ (compare with Fig.3 in Kolawole et al., 2021a). There is possibility of a third RIZ, the Hengshan RIZ, which separates the Datong and Xinding basins. The Hengshan RIZ is an overlapping divergent RIZ and is completely unbreached, therefore it will not be discussed at length in the following. RIZs can also be classified on their evolution stage (from Kolawole et al. 2021a) i.e. whether the RIZ is unbreached, partially breached, recently breached, or breached. This is assessed based on two observations: 1) Presence of a breaching fault that extends from one rift segment to the other segment and 2) Presence of an established physical linkage of depositional environments of both rift segments (i.e. is the drainage between both segments connected). Recently breached and breached RIZs have an established breaching fault and connect the drainage of two different rift segments, but breached RIZs shows less topography due to increased subsidence during the longer time period since the RIZ was breached. Unbreached RIZs show no apparent structural connection and no drainage connection, while partially breached RIZs may have a breaching

fault partially connecting the rift basins but the drainage integration has not occurred yet. The different RIZ stages come with distinct morphological responses and have relevance to the seismic hazard so in the following we classify the two RIZs in the Shanxi Rift based on the Kolawole et al. (2021a) classification scheme and assess the response of the geomorphic indices.
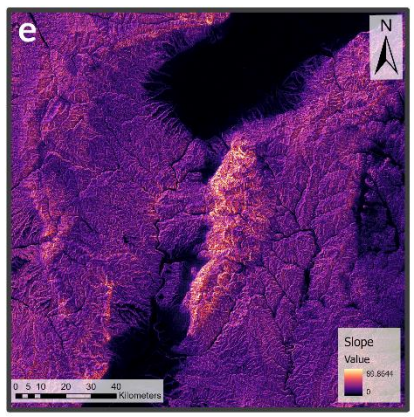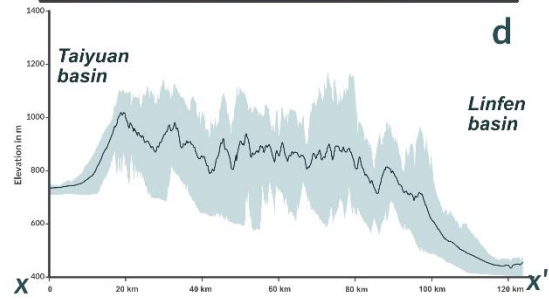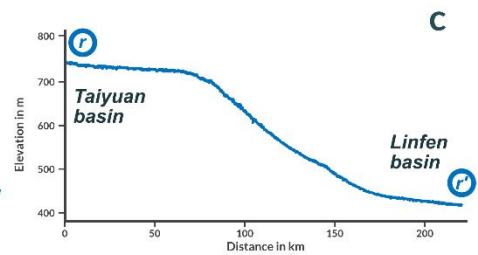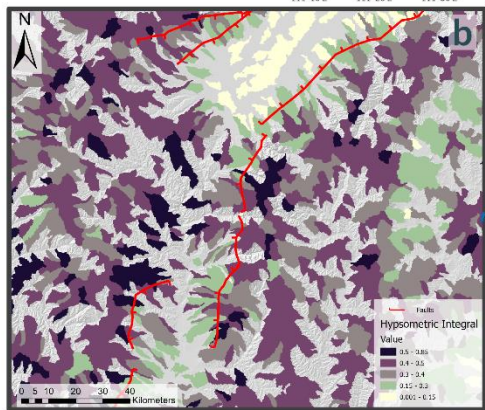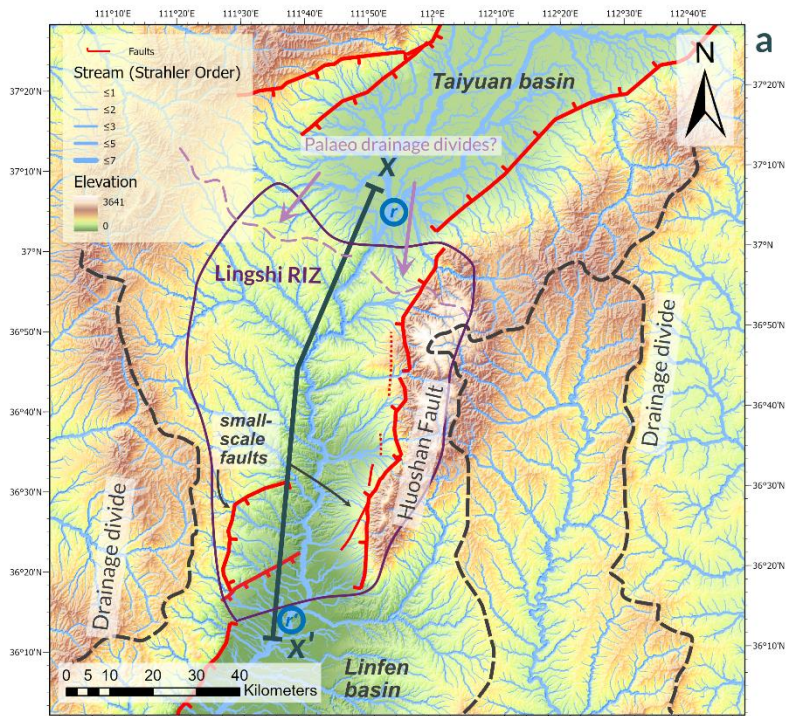
Figure 8: a) Topographic map with drainage (weighted by stream order) showing the drainage divide and reorganisation happening at the Lingshi RIZ. **b)** HI map of the Lingshi RIZ, showing high values in the footwall of the Huoshan Fault but also in the hangingwall. **c)** Longitudinal river profile of the Upper Fen River showing the characteristic "down stepping" shape of river profiles

across recently breached RIZs. d) Swath profile of the Lingshi RIZ, shaded area indicates maximum and minimum elevation in a 5km corridor along the line of section– line of section shown on 7a). e) Slope map of the Lingshi RIZ that shows very high values along the main border fault (Huoshan) but also clear distinct breaks in the SW.

450   The Lingshi RIZ (Fig. 8) is the southernmost RIZ connecting the Taiyuan and Linfen basins. The breaching fault, which in this case is the Huoshan fault, is well developed and has established a physical connection between the Taiyuan and Linfen basin. The Huoshan fault and other small-scale faults within the Lingshi RIZ are shorter, more segmented, and variably oriented compared to the faults of the major subbasins. These small-scale faults are more visible in the slope map (Fig. 8e) as sharp linear breaks. The footwall of the Huoshan fault shows high values of HI in the excess of 0.5 (Fig. 8b) however, the

455 whole RIZ shows high values of HI which are sometimes connected to smaller scale faults, highlighting the complexity and distribution of faulting in the RIZ. As noted in 4.1, loess can have a significant impact on the HI response of a region, therefore the high HI response in the Lingshi RIZ may in part be related to the degree of loess coverage. However, the loess is constrained to the hanging wall of the Huoshan Fault and therefore the high HI response in the Huoshan fault footwall is not influenced by loess. The drainage of the Taiyuan and Linfen basin are connected across the Lingshi RIZ as the Fen River is flowing across

460 it. The drainage was previously not connected as there are possible palaeo-drainage divides (in purple – Fig.8a), where tributaries of streams flow in separate directions. Li et al. (1998) proposed that during the early evolution of the Shanxi Rift in the Miocene and Pliocene, the basins were filled by isolated lakes and later, during the mid-Pleistocene, a fluvial connection was established. Hu et al. (2005) identified three lake terraces in the Taiyuan and Linfen basins, with the latest regression occurring at 0.13 Ma. Based on this the integration and breaching across the Lingshi RIZ likely occurred in the Middle - Late

465 Pleistocene. The swath profile of the RIZ and the longitudinal river profile (8d, e) showing the down stepping morphology that is commonly associated with recently breached RIZs and may be a relic of the lake terraces prior to the fluvial connection being established. As the breaching fault (Huoshan) is well developed and has established a physical connection which has connected the depositional systems of both basins, as well as the characteristic morphology of the Lingshi RIZ, we classify it as a recently breached RIZ.

470

    The Shilingguan RIZ (Fig. 9) separates the Xinding Basin to the north and the Taiyuan Basin to the south. The breaching fault (Shilingguan Fault) is physically connected to the Jiaocheng fault but not to the Xizhoushan fault. The fault itself appears to be segmented as seen by the various orientations of the fault segments (Fig. 9c). The topographic swath profile of the RIZ shows the topographic high stand of the RIZ (Fig. 9d). The footwall of the Shilingguan fault exhibits very high (>0.5) HI

475 values and the Fen River in its footwall is highly sinuous but has high topography, relief, and steep slopes on either side, also known as an entrenched meander (Gardner, 1975; Harden, 1990). Combining all these observations indicates that this area of the Shanxi Rift has experienced recent uplift. The Shilingguan RIZ represents a drainage divide, with the Hutuo River, north of the RIZ is being deflected eastwards and draining across the Xizhoushan fault through the Taihang mountains into the North China Plain (Fig.2). In contrast, the Fen River flows from the NW and crosses the main breaching fault before draining towards

480   the south into the Taiyuan basin. Windgaps (Fig. 9a) in the footwall of the Xizhoushan fault to the east show that possibly the drainage of the Upper Fen River once occurred across this RIZ from west to east before the initiation of the Shilingguan Fault and uplift of its footwall caused the diversion of the river to the south. As the depositional systems of the Xinding and Taiyuan basins are not connected across the RIZ, and the breaching fault has not established a full physical link, this RIZ represents a partially breached RIZ.

485

The different breaching stage of the Lingshi and Shilingguan RIZ may be related to their previously mentioned geometrical arrangement, which led to earlier breaching of the Lingshi RIZ (underlapping oblique convergent RIZ). The influence of initial geometry was shown by Kolawole et al. (2024) in a numerical model of the southern Malawi Rift, where the tip-to-tip arrangement of the Nsanje RIZ favoured rift coalescence compared to the overlapping divergent geometry of the Middle Shire

490   RIZ. The convergent RIZ geometry of the Lingshi RIZ was beneficial for strain localisation and stress concentration at the fault tips of the surrounding basin bounding faults (Jiaocheng and Linfen) while the divergent geometry of the Shilingguan RIZ stalled rift coalescence. This in turn may also explain why the Hengshan RIZ is unbreached as it has an overlapping divergent geometry which is unfavourable to stress concentration and rift coalescence. Breaching status of the RIZs increases towards the south which may be controlled by the different RIZ geometries.

Shilingguan RIZ

partially breached RIZ
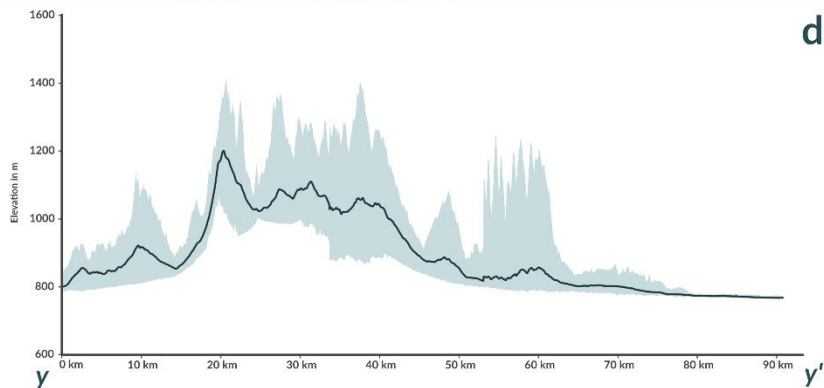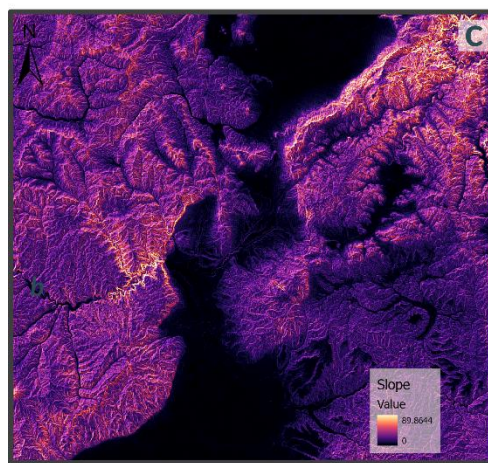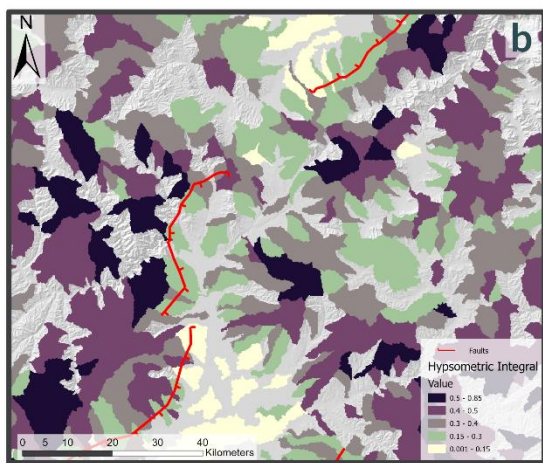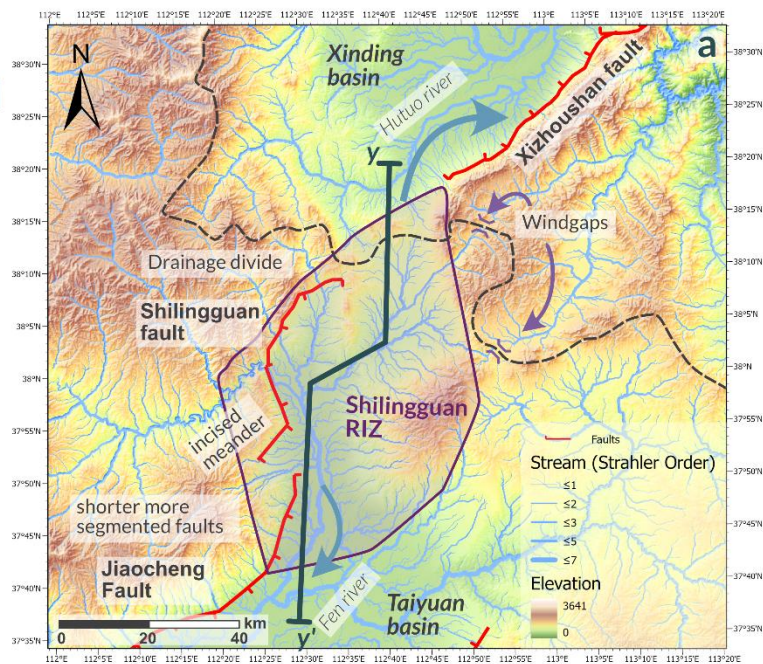
Figure 9: a) Topographic map with streams (weighted by stream order) showing the drainage divide and reorganisation happening at the Shilingguan RIZ. b) HI map of the Shilingguan RIZ, showing the high values in the footwall of the main faults, especially in the Shilingguan fault footwall where the high slope values are found. c) Slope map of the Shilingguan RIZ. High slope values are closely associated with the main faults but can also be seen along the steep sides of the meandering rivers in both the footwall of the Xizhoushan Fault and the Shilingguan Fault. d) Swath profile of the Shilingguan RIZ, shaded area indicates maximum and minimum elevation in a 5km corridor along the line of section – line of section shown in 8a)

Geomorphic evidence shows that the RIZ are currently the most active regions of faulting and reorganisation, as breaching faults of the RIZs (Huoshan, Shilingguan) show consistently high geomorphic values (Table 1; Figure 7). They also show major changes in fault strike compared to the NE-SW trending basins (Fig. 7 and 8). Most faults in the RIZs do not strike NE-SW but show more distributed patterns of N-S and NE-SW striking faults. Commonly an overall "zig-zag pattern" forms, with fault segments of variable direction. Faults oblique to the general extension direction commonly form at the intersection points between major faults. Hodge et al. (2018b) show in models that Coulomb stress changes along the tips of established faults lead to the formation of new off-axis trending faults, with the geometry of these dependent on the lateral separation and amount of under- or overlap of the interacting faults. This process is common in other rift basins across the world (Maerten, 2000; Morley, 2010) and is similar to observations of faults in the RIZs of Shanxi. The N-S striking fault segments in the RIZs show overall higher geomorphic index values compared to the NE-SW trending faults of the sub-basins, suggesting they are more tectonically active as the active deformation is focused along zones of active linkage. The morphology of the N-S faults in the RIZs suggest that they are younger faults which are still early in the reorganisation phase, as they are shorter, more segmented, and often show lower topographic offset. Morphologically more mature NE-SW striking basin bounding faults have lower geomorphic index values than the faults in the RIZs also show high values, especially in the case of the Wutai and Xizhoushan faults. In the Shanxi Rift faults of all orientations may show high activity levels, however faults in the RIZs show the highest activity. This activity pattern is consistent with the idea of an overall stable extension direction (Middleton et al. 2017) where all faults remain possibly active, but activity is concentrated in the linkage zones.

RIZs often experience increased seismic activity due to increased strain along the tips of established basin bounding faults that progressively link across the RIZs. This was observed at the tips of the Rukwa Rift and the Rukwa-Tanganyika RIZ by Kolawole et al. (2021) and Kolawole et al. (2024) as well as for the Turkana Rift (Musila et al., 2023). The breaching faults in the RIZ could have a buffering effect on the NE-SW trending faults of the main sub-basins as the overall strain accommodated across the Shanxi Rift is concentrated on the breaching faults in the RIZs, therefore the longer NE-SW trending faults accommodate overall less strain. Increased strain rate on faults post linkage has been shown to occur both in theory (Cowie et al. 2005) and the Whakatne Graben, NZ (Taylor, 2004). The heightened activity at these RIZs is not only shown by geomorphology but also by seismicity: Chen et al. (2021) processed receiver function data that shows cluster of earthquakes at or near both above-mentioned RIZs, while events in the individual subbasins are more distributed. The ISC catalogue (Storchak et al., 2013; 2015; Di Giacomo et al., 2018) covering earthquakes occurring between 1907 and 2022 (Fig.2) show similar clusters around the RIZ, although the cluster around the Shilingguan RIZ is more pronounced. The faults in the

Shilingguan RIZ are comparatively short and segmented (10-20km), ~~this~~ might limit their ability to generate large magnitude earthquakes. However, the Huoshan Piedmont Fault, the breaching fault of the Lingshi RIZ, is equally segmented (Fig. 7a) with segments 20-30km in length and has shown to be the site of major historic earthquakes. The historic Hongdong Earthquake (M_w 7.2-7.6) in 1303 CE was caused by slip on the Huoshan Piedmont fault (Xu et al. 2018) and had an estimated rupture length of 98km, which shows that multiple segments can link up during seismic slip to generate larger magnitude events. The Shanxi Rift is a low strain rate region, meaning major earthquakes are infrequent but potentially devastating as evidenced by the Hongdong 1303 event (Xu et al. 2018). Overall, the NE-SW trending faults which are longer but potentially less active might be capable of generating larger but more infrequent events (Scholz et al. 1982; Leonard, 2010), while the more segmented faults in the RIZs could produce more frequent yet smaller magnitude earthquakes.

5.3 The role of inheritance in the Shanxi Rift – crust or mantle control?

Most continental rifts are influenced by inherited structures that are either reactivated (Daly et al., 1989; Wheeler and Karson et al., 1989; Holdsworth et al., 2001; Kinabo et al., 2008; Phillips et al., 2016; Wedmore et al., 2020; Kolawole et al., 2021b) or reorientate the rift scale strain field in local areas (Morley, 2010; Philippon et al. 2015; Kolawole et al., 2018; Samsu et al., 2023). The Shanxi Rift exploited rheological weaknesses during its formation at the rift scale (TNCO) and on smaller individual fault scales. At first order, the spatial relationship between the Shanxi Rift and the TNCO is obvious (Fig. 1). The Shanxi Rift is directly superimposed on the Paleoproterozoic orogen (Xu et al., 1993). The TNCO acted as a rheological weakness in comparison to the adjacent stronger Western Block of the NCC and therefore the TNCO was exploited by the Shanxi Rift. Orogenic belts behaving as weak zones for nucleating rifts is a common suggestion (i.e. East Africa (Rosendahl, 1987; Morley, 1988; Daly et al., 1989; Ring, 1994) or Baikal – Petit et al., 1996). In Shanxi, faults often define the edges of Paleoproterozoic basement complexes and expose these at the surface by footwall uplift (e.g. Wutai, Hengshan, Xizhoushan, Zhongtiaoshan). Some of the rift faults do not contain Precambrian crystalline rocks in the footwall, but for example the Jiaocheng and Taigu faults are in the direct vicinity of the crystalline Lüliangshan and Taihangshan massif (about 50km distance). Basement complexes such as the Huoshan, Fuping or Lüliangshan are also cored by Precambrian granitic plutons which formed as late orogenic intrusions during the TNCO formation. These stronger more buoyant granitic blocks may have been more resistant to deformation hence the rift faults preferentially formed along the pluton margins and are uplifted within the fault footwall. This is similar to observations from offshore New Zealand (Phillips and McCaffrey, 2019; Phillips et al. 2023) or Carboniferous rift systems of the United Kingdom (Fraser and Gawthorpe, 1990; Howell et al., 2020).

The similar trends of ancient pre-existing structures and active extensional faults show that the Paleoproterozoic fabrics of the TNCO potentially influence the orientation of the active faults of the Shanxi Graben. Major NE-SW trending basin bounding faults in the Shanxi Rift (Wutai, Xizhoushan, Taigu, Jiaocheng, Zhongtiaoshan) are generally parallel to inherited NE-SW (45-55°) trending Paleoproterozoic basement fabrics (Fig. 5). The Wutai and Zhongtiaoshan faults all strike ENE-WSW (60-70°), matching the trend of the inherited structures in the footwall of these faults. Therefore, it is likely that crustal structures

565 influenced the orientation of these faults. The Hengshan fault locally trends parallel to the basement fabrics but often strikes obliquely and cuts across some of the shallow basement fabrics observed at surface. It is possible that it locally exploits the shallow basement fabrics while following the trend of a deeper-seated weakness that is oblique to the shallow basement fabrics observed at surface, similar to the Bilila-Mtakataka Fault (Hodge et al. 2018a) in Malawi. The Xizhoushan fault follows the trend of the fabrics in the western part of the Fuping complex. There is a major crustal boundary running through the Fuping

570 complex which is known as the Longquanguang fault (LGQF) which is a gently dipping ductile thrust fault, according to Trap et al. (2012). To the southeast of the LGQF there is a major change in trend of the Palaeoproterozoic fabrics to a generally NW-SE/E-W direction (compare stereonets of Fuping-West and Fuping-East on Fig. 5). The crustal structures of the eastern Fuping Block have no influence on the Xizhoushan fault (or any other fault in the Shanxi Rift), possibly because the LGQF represents a mechanical barrier. The Xizhoushan fault may merge with the LQGF at depth; however, this is mostly speculation

575 based on their matching orientation and proximity. Merging of faults on shallower dipping structures has been observed by Phillips et al. (2016) in the North Sea. The long (>50km) basin bounding faults of the Shanxi Rift nucleated along preferentially orientated inherited fabrics of the Palaeoproterozoic basement complexes which may have aided with early fault nucleation similar to observations in other global rift systems (Phillips et al., 2016; Rotevatn et al., 2018; Heilman et al. 2019; Collanega et al., 2019; Vasconcelos et al., 2019; Ramos et al., 2022)

580

Faults in the RIZs show a more disconnected pattern (Figs. 8, 9), vary more in orientation (N-S and NE-SW) and are shorter (10-30km) than the long NE-SW trending basin bounding faults (up to 100km). Individual fault segments in the RIZs alternate between following the crustal inherited fabric, which broadly trends NE-SW, and cutting across the fabric and striking more N-S or NNE-SSW. As RIZ faults mature, segments link up and grow into one throughgoing structure that has a "zig-zag"

585 pattern that cuts across pre-existing fabrics, this is especially visible on plan-view of the Huoshan Piedmont Fault (Fig. 8). These "zig-zag" patterns in faults have been observed in various other rifts such as offshore West Greenland (Peace et al., 2018, Schiffer et al., 2020), the North Sea (Henza et al. 2011; Henstra et al., 2015) and the main Ethiopian Rift (Moore and Davidson, 1978; Vetel and Le Gall, 2006; Corti et al., 2022; Lezzar et al., 2002; Corti, 2009; Hodge et al., 2018a). In the case of Greenland and Ethiopia, rifting was oblique to major basement shear zones which lead to the formation of two sets of faults

590 with some of them parallel to the extension direction and others parallel to the inherited structures. In the Shanxi Rift the regional NW-SE extensional vector (Middleton et al. 2017) is likely perturbed around the RIZs due to interactions of the fault tips of the adjacent basin-bounding faults. The resulting strain field would be oblique to the inherited structures. This results in the formation of N-S trending faults perpendicular to the perturbed strain field cutting across the inherited basement fabrics as well as NE-SW trending faults following the trend of pre-existing Proterozoic structures. Therefore, as the faults grow and

595 coalesce across the RIZs they will both cut across or locally exploit the inherited fabrics (Heilman et al., 2019; Kolawole et al. 2021), resulting in the observed zig-zag fault pattern. Fault geometry may also be controlled by multiple levels of inheritance as observed by Wedmore et al. (2020) for the Thyolo Fault in Malawi and Hodge et al. (2018a) for the Bilila-Mtakataka Fault, where shallow level structures control the surface geometry of the fault, but a deeper-seated weakness controls the overall

orientation which is oblique to the overall strain field. We consider the possibility that the NE-SW trending faults in the RIZs formed parallel to inherited fabrics early and later were linked up by N-S trending segments. This behaviour was observed on the Norwegian Margin of the North Sea by Henstra et al. (2015) where early rift faults from a E-W orientated phase of rifting influenced the location and morphology of later rift faults during a subsequent phase of rifting, which was orientated obliquely to the early faults. However, we did not find major morphological or geomorphological value differences between the N-S and NE-SW trending faults that would suggest that one set formed earlier, therefore it is possible that they are co-eval.
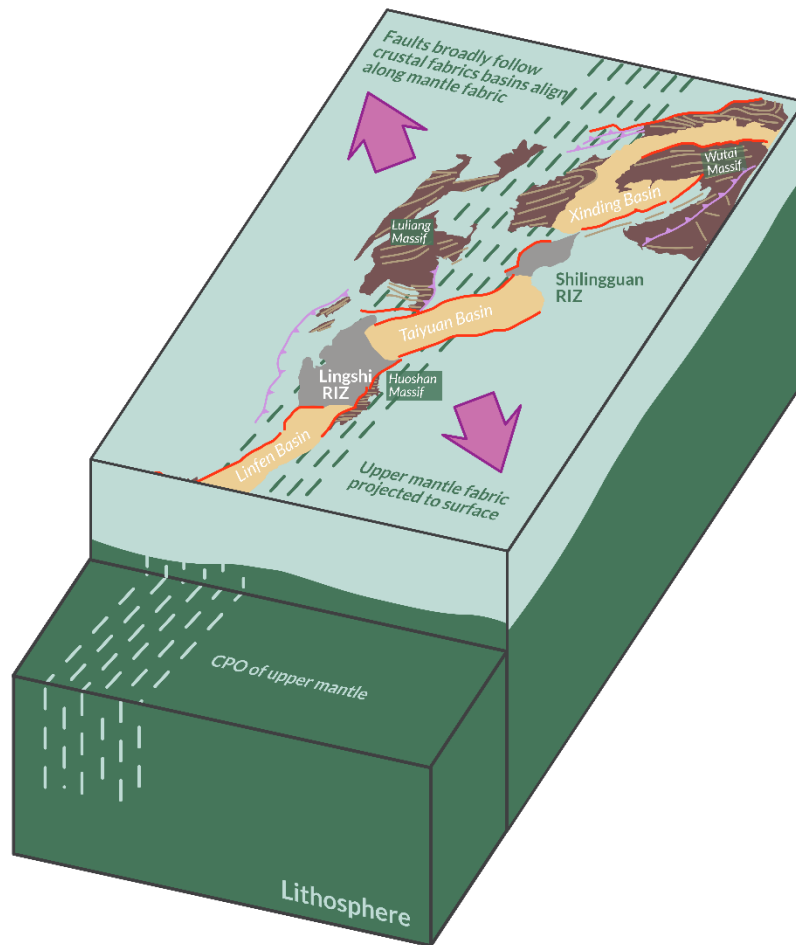
Figure 10: Schematic 3D diagram of the Shanxi Rift showing the proposed obliquity between mantle anisotropy and crustal inherited fabrics. Mantle anisotropy is defined by the suggested crystal preferred orientation (evidenced by shear wave splitting data (Zhao and Zheng, 2005)) in the upper mantle, that broadly trends N-S, while the crustal fabrics trend NE-SW. The Shanxi Rift basins are collated with a zone of aligned mantle fabric which is oblique to the principal extension direction (indicated as purple arrows). Individual basins and their bounding faults formed parallel to inherited crustal fabrics. This creates the characteristic en-echelon pattern of Shanxi Rift.

The N-S and NE-SW trends of faults found at local scale in the RIZs ~~are~~ can also be observed for the entire Shanxi Rift. The Shanxi Rift is an S-shaped en-echelon rift that follows a broad N-S trend with individual basins and their bounding-faults oriented NE-SW. While the TNCO broadly trends N-S or NNE-SSW (Fig. 1; Zhao et al., 2005), the individual crustal structures such as major shear zones, thrust faults or fabrics broadly trend NE-SW (Fig. 10). A broadly NNE-SSW to N-S trending anisotropy (0-15°) in the upper mantle of the Central Zone of the North China Craton is shown by shear wave splitting data from the upper mantle (Chen, 2010, Zhao and Zheng, 2005). The apparent obliquity between the trend of crustal structures and the upper mantle fabric shows that crustal inheritance and the lithospheric inheritance may not share a common orientation, which is a common feature of many rift zones (Vauchez et al., 1997; Tomassi and Vauchez, 2001). Recent analogue modelling of oblique crustal and mantle fabrics by Zwaan et al. (2022) show similar patterns to those observed in the Shanxi Rift. Analogue modelling by Molnar et al. (2020) show that lithospheric weaknesses influence the rift trend while oblique crustal structures segment the rift at a local scale. The difference in lithospheric and crustal structural trends could have either occurred during transpressional accretion of the TNCO, such as proposed by Li et al. (2010) where subduction occurred along a N-S trend while the later collision that formed the TNCO formed NE-SW trending fabrics. It may have also formed during later reworking by the polyorogenic event that formed the TNCO, where the N-S trending TNCO was partially reworked by a collision of the Columbia supercontinent in the Palaeoproterozoic which resulted in the formation of the E-W trending Inner Mongolia – North Hebei Orogen (Kusky & Li, 2003; Kusky et al. 2007; Santosh, 2010). However, the evolutionary history of the TNCO is debated and resolution of the exact timing of events is beyond the scope of this paper. Mesozoic compression across North China, commonly known as the Yanshanian orogeny (Zhang et al., 2008; Zhang et al., 2011; Clinkscales and Kapp, 2019) has also affected the Shanxi region and may have also caused further reworking of the TNCO and rotated the crustal fabrics to the present-day orientation. Determining the exact reason for the apparent obliquity between crustal and lithospheric trends of the TNCO is not resolvable in this study and would require further work. The principal extension direction determined by Middleton et al. (2017) of 151° for the Shanxi Rift is roughly perpendicular to the inherited structures in the crust but oblique to the proposed broad upper mantle anisotropy, which resulted in the early rift basins exploiting the favourably orientated crustal fabrics while the general trend of the rift is oblique to the extension direction along an upper mantle fabric that created a rheological weakness. This en-echelon arrangement of rift basins above a broad oblique deep seated weak zone has been shown in analogue models by D'Agostini (2009), showing similar geometries as exhibited by the Shanxi Rift. However, we acknowledge that the observed mantle anisotropy may not be an inherited mantle fabric and could have formed during rifting (Gao et al., 1997; Kendall et al. 2006) and is aligned oblique to the rift (Tepp et al., 2018; Ebinger et al., 2024). Thus, the mantle fabric underlying Shanxi may be Cenozoic in age formed during extensional deformation of North China as has been proposed previously (Chang et al., 2012). We emphasise that our interpretation that the Shanxi Rift architecture is influenced by a crustal and mantle fabrics of the TNCO that are oblique to each other is speculative.

We propose a new model for the evolution of the Shanxi Rift that incorporates a heterogenous basement with inherited structures. This model is consistent with our geomorphic results (Fig. 11) and can explain the evolution of the Shanxi Rift under a constant strain field, making it simpler than, frequent changes in the strain field (Shi et al., 2015a; Shi et al., 2020;

Assie et al., 2022). In our model, the extensional strain field trends NW-SE which is consistent with previous estimations of the present-day extensional strain field using GPS or seismicity data (Middleton et al., 2017; Shen et al., 2000). However, locally the strain is reorientated either by inherited structures (i.e., Wutai and Zhongtiaoshan (Fig. 9)) or interactions between

650 basin-bounding faults that rotate the local strain field in the RIZs between them (Shilingguan and Lingshi). This means that there is no specific set of faults that is favoured by changes of strain fields therefore potentially all faults remain active, yet there are certain faults that are more active due active reorganisation and linkage in RIZs. Faults established early on along preferentially aligned NE-SW trending inherited structures and formed the major basins: Taiyuan, Xinding and Linfen. These basins formed in an en-echelon arrangement along a N-S trending upper mantle structure (Fig. 10 and 11). As the faults and

655 basins grew, they started interacting and linking across topographical high stands that saw less faulting and subsidence - the RIZs. These RIZs have a more complex faulting pattern as the interacting faults create a locally rotated strain field which is oblique to the crustal structures and the regional strain field. This creates a "zig-zag geometry" as the shorter fault segments grow and coalesce. As linkage progresses, these RIZs link the different basins and establish physical and sedimentary system links. This linkage is ongoing to the current day, as represented by the only partially breached RIZ of Shilingguan.

660

Fig. 11. The new proposed evolutionary model under a constant strain field that shows linkage of rift basins influenced by two levels of inheritance – crustal and mantle inheritance which result in oblique rifting and the creation of en-echelon array of basins. Crustal fabrics aid strain accommodation and influence geometry of linkage faults in the RIZs.

6 Conclusions

We applied geomorphic indices to the Shanxi Rift to understand the role structural inheritance has played in the evolution of the rift systems and the seismic hazard posed by active faults within it. We have shown that geomorphic indices are a powerful tool to evaluate the evolution and segmentation of the Shanxi Rift. Our study shows that lithology has a strong influence on the overall geomorphic signal of faults, as those with Paleoproterozoic crystalline basement in their footwalls have overall higher geomorphic values compared to faults with Palaeozoic-Mesozoic metasediments in the footwalls. However, comparing faults with similar basement geology can circumvent this problem. We found that overall HI is less sensitive to these variations of lithology compared to Relief and k_{sn}. Therefore, HI may be more suited to evaluating the tectonic influence on landscapes. The geomorphic analysis showed that in the Shanxi Rift, the RIZs that link the established large basins, namely the Xinding and Taiyuan basins, are the most active zones and show most signs of active drainage reorganisation. This has major implications for seismic hazard assessments as it hints towards zones which show more complex and more active patterns of faulting due to the strain concentration in the RIZs, these may experience increased seismicity. Linkage of the basins seems to be progressing towards the north as shown by the increasing breaching status of the RIZs towards the south, the breaching status of the RIZ is possibly controlled by their initial geometry.

Structural inheritance played a key role in the evolution and segmentation of the Shanxi Rift. The collision of the two component blocks of the NCC created a lithospheric scale weak zone, the TNCO, which preferentially accommodates strain as it is more easily deformed than the surrounding cratonic area. The individual sub-basins of the Shanxi Rift align form en-echelon a broad N-S trend which coincides with an upper mantle anisotropy fabric – a lithospheric manifestation of the TNCO. Inherited fabrics in the upper crust are orientated NE-SW, perpendicular to the regional extension direction. The extension direction is oblique to the assumed upper mantle inherited fabric which, causes the en-echelon pattern of individual rift basins. Early rift faults nucleated along NE-SW orientated basement fabrics, establishing basins arranged along the inherited N-S trend. As the boundary faults grew, they began to interact and form RIZs. Within these RIZs, the crustal basement inheritance further influenced and segmented the breaching faults and aided linkage across the basins. The faults within them both follow and crosscut pre-existing fabrics in the crust creating a "zig-zag pattern" of small, segmented faults that eventually link up into singular throughgoing fault zones. Therefore, structural inheritance of pre-existing Precambrian basement fabrics and a locally rotated stress field resulted in the complex pattern of faulting we now see in the RIZs. Thus, frequent changes of the extensional vector are not needed to explain the evolution of the Shanxi Rift as data is consistent with an evolution under a constant strain field. We propose that the Shanxi Rift is a type-example of an oblique rift that is influenced by an inheritance at different scales, as upper mantle, and crustal basement fabrics as well as pre-existing faults have influenced the pattern of faulting observed today.

Data availability

695 A geopackage of the GIS project with the associated raster files of the geomorphic indices is available on the Zenodo repository associated with this publication (https://doi.org/10.5281/zenodo.7317598, Phillips et al., 2022). These can be opened with QGIS. The R code for calculating the Hypsometric integral is available on GitHub: (https://github.com/MFroemchen/R_Hypsometry)

Author contributions

700 MF, KJWM, MBA, JVH and TBP conceptualised the study. MF undertook the geomorphic and structural analysis. MF prepared the manuscript and figures along with input from KJWM, MBA, JVH, and all other co-authors. All co-authors contributed to writing, revising, and preparing of the manuscript.

Competing interests

705 The contact author has declared that none of the authors has any competing interests.

Financial support

This research has been supported by the Natural Environment Research Council (grant no. NE/S007431/1).

References

Aanyu, K. and Koehn, D.: Influence of pre-existing fabrics on fault kinematics and rift geometry of interacting segments:
710 Analogue models based on the Albertine Rift (Uganda), Western Branch-East African Rift System, Journal of African Earth Sciences, 59, 168–184, https://doi.org/10.1016/j.jafrearsci.2010.10.003, 2011.

Agostini, A., Bonini, M., Corti, G., Sani, F., and Mazzarini, F.: Fault architecture in the Main Ethiopian Rift and comparison with experimental models: Implications for rift evolution and Nubia–Somalia kinematics, Earth and Planetary Science Letters, 301, 479–492, https://doi.org/10.1016/j.epsl.2010.11.024, 2011.

715 Ahnert, F.: Functional relationships between denudation, relief, and uplift in large, mid-latitude drainage basins, American Journal of Science, 268, 243–263, https://doi.org/10.2475/ajs.268.3.243, 1970.

Ai, S., Zheng, Y., He, L., and Song, M.: Joint inversion of ambient noise and earthquake data in the Trans-North China Orogen: On-going lithospheric modification and its impact on the Cenozoic continental rifting, Tectonophysics, 763, 73–85, https://doi.org/10.1016/j.tecto.2019.05.003, 2019.

720 Allen, M. B., Macdonald, D. I. M., Xun, Z., Vincent, S. J., and Brouet-Menzies, C.: Early Cenozoic two-phase extension and late Cenozoic thermal subsidence and inversion of the Bohai Basin, northern China, Marine and Petroleum Geology, 14, 951–972, https://doi.org/10.1016/S0264-8172(97)00027-5, 1997.

Assie, K. R., Wang, Y., Tranos, M. D., Ma, H., Kouamelan, K. S., Brantson, E. T., Zhou, L., and Ketchaya, Y. B.: Late Cenozoic faulting deformation of the Fanshi Basin (northern Shanxi rift, China), inferred from palaeostress

725 analysis of mesoscale fault-slip data, Geological Magazine, 1–17, https://doi.org/10.1017/S0016756822000085, 2022.

Brune, S., Corti, G., and Ranalli, G.: Controls of inherited lithospheric heterogeneity on rift linkage: Numerical and analog models of interaction between the Kenyan and Ethiopian rifts across the Turkana depression, Tectonics, 36, 1767–1786, https://doi.org/10.1002/2017TC004739, 2017.

730 Bull, W. B. and McFadden, L. D.: Tectonic Geomorphology North and South of the Garlock Fault, California, in: Geomorphology in Arid Regions, Routledge, 1980.

Chang, L., Wang, C.-Y., and Ding, Z.: Upper mantle anisotropy beneath North China from shear wave splitting measurements, Tectonophysics, 522–523, 235–242, https://doi.org/10.1016/j.tecto.2011.12.009, 2012.

Chen, G.: On the geotectonic nature of the Fen-Wei rift system, Tectonophysics, 143, 217–223,

735 https://doi.org/10.1016/0040-1951(87)90091-6, 1987.

Chen, L.: Concordant structural variations from the surface to the base of the upper mantle in the North China Craton and its tectonic implications, Lithos, 120, 96–115, https://doi.org/10.1016/j.lithos.2009.12.007, 2010.

Chen, W.-P. and Nábelek, J.: Seismogenic strike-slip faulting and the development of the North China Basin, Tectonics, 7, 975–989, https://doi.org/10.1029/TC007i005p00975, 1988.

740 Chen, Y., Chen, J., Li, S., Yu, Z., Liu, X., and Shen, X.: Variations of crustal thickness and average Vp/Vs ratio beneath the Shanxi Rift, North China, from receiver functions, Earth, Planets and Space, 73, 200, https://doi.org/10.1186/s40623-021-01528-8, 2021.

Chen, Y.-C., Sung, Q., and Cheng, K.-Y.: Along-strike variations of morphotectonic features in the Western Foothills of Taiwan: tectonic implications based on stream-gradient and hypsometric analysis, Geomorphology, 56, 109–137,

745 https://doi.org/10.1016/S0169-555X(03)00059-X, 2003.

Clinkscales, C. and Kapp, P.: Structural style and kinematics of the Taihang-Luliangshan fold belt, North China: Implications for the Yanshanian orogeny, Lithosphere, 11, 767–783, https://doi.org/10.1130/L1096.1, 2019.

Clinkscales, C., Kapp, P., Thomson, S., Wang, H., Laskowski, A., Orme, D. A., and Pullen, A.: Regional exhumation and tectonic history of the Shanxi Rift and Taihangshan, North China, Tectonics, 40, e2020TC006416, 2021.

750 Collanega, L., Siuda, K., A.-L. Jackson, C., Bell, R. E., Coleman, A. J., Lenhart, A., Magee, C., and Breda, A.: Normal fault growth influenced by basement fabrics: The importance of preferential nucleation from pre-existing structures, Basin Research, 31, 659–687, https://doi.org/10.1111/bre.12327, 2019.

Corti, G.: Continental rift evolution: From rift initiation to incipient break-up in the Main Ethiopian Rift, East Africa, Earth-Science Reviews, 96, 1–53, https://doi.org/10.1016/j.earscirev.2009.06.005, 2009.

755   Corti, G., Iandelli, I., and Cerca, M.: Experimental modeling of rifting at craton margins, Geosphere, 9, 138–154, https://doi.org/10.1130/GES00863.1, 2013.

Corti, G., Maestrelli, D., and Sani, F.: Large-to Local-Scale Control of Pre-Existing Structures on Continental Rifting: Examples From the Main Ethiopian Rift, East Africa, Frontiers in Earth Science, 10, 2022.

Cowie, P. A., Underhill, J. R., Behn, M. D., Lin, J., and Gill, C. E.: Spatio-temporal evolution of strain accumulation

760   derived from multi-scale observations of Late Jurassic rifting in the northern North Sea: A critical test of models for lithospheric extension, Earth and Planetary Science Letters, 234, 401–419, https://doi.org/10.1016/j.epsl.2005.01.039, 2005.

Cox, R. T.: Analysis of drainage-basin symmetry as a rapid technique to identify areas of possible Quaternary tilt-block tectonics: An example from the Mississippi Embayment, GSA Bulletin, 106, 571–581,

765   https://doi.org/10.1130/0016-7606(1994)106<0571:AODBSA>2.3.CO;2, 1994.

Crider, J. G. and Pollard, D. D.: Fault linkage: Three-dimensional mechanical interaction between echelon normal faults, Journal of Geophysical Research: Solid Earth, 103, 24373–24391, https://doi.org/10.1029/98JB01353, 1998.

Daly, M. C., Chorowicz, J., and Fairhead, J. D.: Rift basin evolution in Africa: the influence of reactivated steep basement shear zones, Geological Society, London, Special Publications, 44, 309–334,

770   https://doi.org/10.1144/GSL.SP.1989.044.01.17, 1989.

Davis, G., Zheng, Y., Cong, W., Darby, B., Zhang, C., and Gehrels, G.: Mesozoic tectonic evolution of the Yanshan fold and thrust belt, with emphasis on Hebei and Liaoning provinces, northern China, in: Geol. Soc. Am. Mem., vol. 194, 171–197, https://doi.org/10.1130/0-8137-1194-0.171, 2001.

Deng, Q., Ran, Y., Yang, X., Min, W., and Chu, Q.: Map of Active tectonics in China, Seismological Press, Beijing, 2007.

775   Densmore, A. L., Dawers, N. H., Gupta, S., Allen, P. A., and Gilpin, R.: Landscape evolution at extensional relay zones, Journal of Geophysical Research: Solid Earth, 108, https://doi.org/10.1029/2001JB001741, 2003.

Densmore, A. L., Dawers, N. H., Gupta, S., Guidon, R., and Goldin, T.: Footwall topographic development during continental extension, Journal of Geophysical Research: Earth Surface, 109, https://doi.org/10.1029/2003JF000115, 2004.

780   Di Giacomo, D., Engdahl, E. R., and Storchak, D. A.: The ISC-GEM Earthquake Catalogue (1904–2014): status after the Extension Project, Earth Syst. Sci. Data, 10, 1877–1899, https://doi.org/10.5194/essd-10-1877-2018, 2018.

DiBiase, R. A., Whipple, K. X., Heimsath, A. M., and Ouimet, W. B.: Landscape form and millennial erosion rates in the San Gabriel Mountains, CA, Earth and Planetary Science Letters, 289, 134–144, https://doi.org/10.1016/j.epsl.2009.10.036, 2010.

785   Dong, S., Zhang, Y., Zhang, F., Cui, J., Chen, X., Zhang, S., Miao, L., Li, J., Shi, W., Li, Z., Huang, S., and Li, H.: Late Jurassic–Early Cretaceous continental convergence and intracontinental orogenesis in East Asia: A synthesis of the

Yanshan Revolution, Journal of Asian Earth Sciences, 114, 750–770, https://doi.org/10.1016/j.jseaes.2015.08.011, 2015.

Dulanya, Z., Gallen, S. F., Kolawole, F., Williams, J. N., Wedmore, L. N. J., Biggs, J., and Fagereng, Å.: Knickpoint morphotectonics of the Middle Shire River basin: Implications for the evolution of rift interaction zones, Basin Research, 34, 1839–1858, https://doi.org/10.1111/bre.12687, 2022.

Dunbar, J. A. and Sawyer, D. S.: Continental rifting at pre-existing lithospheric weaknesses, Nature, 333, 450–452, https://doi.org/10.1038/333450a0, 1988.

Ebinger, C. J., Rosendahl, B. R., and Reynolds, D. J.: Tectonic model of the Malaŵi rift, Africa, Tectonophysics, 141, 215–235, https://doi.org/10.1016/0040-1951(87)90187-9, 1987.

Ebinger, C. J., Reiss, M. C., Bastow, I., and Karanja, M. M.: Shallow sources of upper mantle seismic anisotropy in East Africa, Earth and Planetary Science Letters, 625, 118488, https://doi.org/10.1016/j.epsl.2023.118488, 2024.

Erbello, A., Melnick, D., Zeilinger, G., Bookhagen, B., Pingel, H., and Strecker, M. R.: Geomorphic expression of a tectonically active rift-transfer zone in southern Ethiopia, Geomorphology, 403, 108162, https://doi.org/10.1016/j.geomorph.2022.108162, 2022.

Farangitakis, G. P., Heron, P. J., McCaffrey, K. J. W., van Hunen, J., and Kalnins, L. M.: The impact of oblique inheritance and changes in relative plate motion on the development of rift-transform systems, Earth and Planetary Science Letters, 541, 116277, https://doi.org/10.1016/j.epsl.2020.116277, 2020.

Faulds, J. E. and Varga, R. J.: The role of accommodation zones and transfer zones in the regional segmentation of extended terranes, in: Accommodation zones and transfer zones; the regional segmentation of the Basin and Range Province, vol. 323, edited by: Faulds, J. E. and Stewart, J. H., Geological Society of America, 0, https://doi.org/10.1130/0-8137-2323-X.1, 1998.

Faure, M., Trap, P., Lin, W., Monié, P., and Bruguier, O.: Polyorogenic evolution of the Paleoproterozoic Trans-North China Belt—New insights from the Lüliangshan-Hengshan-Wutaishan and Fuping massifs, Episodes Journal of International Geoscience, 30, 96–107, 2007.

Fazlikhani, H., Fossen, H., Gawthorpe, R. L., Faleide, J. I., and Bell, R. E.: Basement structure and its influence on the structural configuration of the northern North Sea rift, Tectonics, 36, 1151–1177, https://doi.org/10.1002/2017TC004514, 2017.

Fick, S. E. and Hijmans, R. J.: WorldClim 2: new 1-km spatial resolution climate surfaces for global land areas, International Journal of Climatology, 37, 4302–4315, https://doi.org/10.1002/joc.5086, 2017.

Fisher, J. A., Pazzaglia, F. J., Anastasio, D. J., and Gallen, S. F.: Linear Inversion of Fluvial Topography in the Northern Apennines: Comparison of Base-Level Fall to Crustal Shortening, Tectonics, 41, e2022TC007379, https://doi.org/10.1029/2022TC007379, 2022.

Flint, J.-J.: Stream gradient as a function of order, magnitude, and discharge, Water Resources Research, 10, 969–973, 1974.

Fossen, H. and Rotevatn, A.: Fault linkage and relay structures in extensional settings—A review, Earth-Science Reviews, 154, 14–28, https://doi.org/10.1016/j.earscirev.2015.11.014, 2016.

Fraser, A. J. and Gawthorpe, R. L.: Tectono-stratigraphic development and hydrocarbon habitat of the Carboniferous in northern England, Geological Society, London, Special Publications, 55, 49–86, https://doi.org/10.1144/GSL.SP.1990.055.01.03, 1990.

Gallen, S. F. and Fernández-Blanco, D.: A New Data-Driven Bayesian Inversion of Fluvial Topography Clarifies the Tectonic History of the Corinth Rift and Reveals a Channel Steepness Threshold, Journal of Geophysical Research: Earth Surface, 126, e2020JF005651, https://doi.org/10.1029/2020JF005651, 2021.

Gao, M., Zeilinger, G., Xu, X., Tan, X., Wang, Q., and Hao, M.: Active tectonics evaluation from geomorphic indices for the central and the southern Longmenshan range on the Eastern Tibetan Plateau, China, Tectonics, 35, 1812–1826, https://doi.org/10.1002/2015TC004080, 2016.

Gao, S., Davis, P. M., Liu, H., Slack, P. D., Rigor, A. W., Zorin, Y. A., Mordvinova, V. V., Kozhevnikov, V. M., and Logachev, N. A.: SKS splitting beneath continental rift zones, Journal of Geophysical Research: Solid Earth, 102, 22781–22797, https://doi.org/10.1029/97JB01858, 1997.

Gao, S., Rudnick, R. L., Carlson, R. W., McDonough, W. F., and Liu, Y.-S.: Re–Os evidence for replacement of ancient mantle lithosphere beneath the North China craton, Earth and Planetary Science Letters, 198, 307–322, https://doi.org/10.1016/S0012-821X(02)00489-2, 2002.

Gao, S., Rudnick, R. L., Yuan, H.-L., Liu, X.-M., Liu, Y.-S., Xu, W.-L., Ling, W.-L., Ayers, J., Wang, X.-C., and Wang, Q.-H.: Recycling lower continental crust in the North China craton, Nature, 432, 892–897, https://doi.org/10.1038/nature03162, 2004.

Gardner, T. W.: The History of Part of the Colorado River and Its Tributaries: An Experimental Study, 87–95, 1975.

Gawthorpe, R. L. and Hurst, J. M.: Transfer zones in extensional basins: their structural style and influence on drainage development and stratigraphy, Journal of the Geological Society, 150, 1137–1152, https://doi.org/10.1144/gsjgs.150.6.1137, 1993.

Gawthorpe, R. L. and Leeder, M. R.: Tectono-sedimentary evolution of active extensional basins, Basin Research, 12, 195–218, https://doi.org/10.1111/j.1365-2117.2000.00121.x, 2000.

Geurts, A. H., Whittaker, A. C., Gawthorpe, R. L., and Cowie, P. A.: Transient landscape and stratigraphic responses to drainage integration in the actively extending central Italian Apennines, Geomorphology, 353, 107013, https://doi.org/10.1016/j.geomorph.2019.107013, 2020.

Goldsworthy, M. and Jackson, J.: Active normal fault evolution in Greece revealed by geomorphology and drainage patterns, Journal of the Geological Society, 157, 967–981, https://doi.org/10.1144/jgs.157.5.967, 2000.

Griffin, B., Andi, Z., O'Reilly, S., and Ryan, C.: Phanerozoic evolution of the lithosphere beneath the Sino-Korean craton: Conference on Mantle Dynamics and Plate Interactions in East Asia, Mantle dynamics and plate interactions in east Asia, 107–126, 1998.

855 Groves, K., Saville, C., Hurst, M. D., Jones, S. J., Song, S., and Allen, M. B.: Geomorphic expressions of collisional tectonics in the Qilian Shan, north eastern Tibetan Plateau, Tectonophysics, 788, 228503, https://doi.org/10.1016/j.tecto.2020.228503, 2020.

Hack, J. T.: Studies of longitudinal stream profiles in Virginia and Maryland, US Government Printing Office, 1957.

Hamdouni, R., Irigaray, C., Castillo, T., Chacón, J., and Keller, E.: Assessment of relative active tectonics, southwest
860 border of the Sierra Nevada (southern Spain), Geomorphology, 150–173, https://doi.org/10.1016/j.geomorph.2007.08.004, 2008.

Harden, D. R.: Controlling factors in the distribution and development of incised meanders in the central Colorado Plateau, GSA Bulletin, 102, 233–242, https://doi.org/10.1130/0016-7606(1990)102<0233:CFITDA>2.3.CO;2, 1990.

He, J., Liu, M., and Li, Y.: Is the Shanxi rift of northern China extending?, Geophysical research letters, 30, 2003.

865 Heilman, E., Kolawole, F., Atekwana, E. A., and Mayle, M.: Controls of Basement Fabric on the Linkage of Rift Segments, Tectonics, 38, 1337–1366, https://doi.org/10.1029/2018TC005362, 2019.

Henstra, G. A., Rotevatn, A., Gawthorpe, R. L., and Ravnås, R.: Evolution of a major segmented normal fault during multiphase rifting: The origin of plan-view zigzag geometry, Journal of Structural Geology, 74, 45–63, https://doi.org/10.1016/j.jsg.2015.02.005, 2015.

870 Henza, A. A., Withjack, M. O., and Schlische, R. W.: How do the properties of a pre-existing normal-fault population influence fault development during a subsequent phase of extension?, Journal of Structural Geology, 33, 1312–1324, https://doi.org/10.1016/j.jsg.2011.06.010, 2011.

Heron, P. J., Peace, A. L., McCaffrey, K. J. W., Welford, J. K., Wilson, R., van Hunen, J., and Pysklywec, R. N.: Segmentation of Rifts Through Structural Inheritance: Creation of the Davis Strait, Tectonics, 38, 2411–2430,
875 https://doi.org/10.1029/2019TC005578, 2019.

Hodge, M., Fagereng, Å., Biggs, J., and Mdala, H.: Controls on early-rift geometry: New perspectives from the Bilila-Mtakataka Fault, Malawi, Geophysical Research Letters, 45, 3896–3905, 2018a.

Hodge, M., Fagereng, Å., and Biggs, J.: The Role of Coseismic Coulomb Stress Changes in Shaping the Hard Link Between Normal Fault Segments, Journal of Geophysical Research: Solid Earth, 123, 797–814,
880 https://doi.org/10.1002/2017JB014927, 2018b.

Holdsworth, R. E., Stewart, M., Imber, J., and Strachan, R. A.: The structure and rheological evolution of reactivated continental fault zones: a review and case study, Geological Society, London, Special Publications, 184, 115–137, https://doi.org/10.1144/GSL.SP.2001.184.01.07, 2001.

Howell, L., Egan, S., Leslie, G., Clarke, S., Mitten, A., and Pringle, J.: The influence of low-density granite bodies on
885 extensional basins, Geology Today, 36, 22–26, https://doi.org/10.1111/gto.12297, 2020.

Hu, X., Li, Y., and Yang, J.: Quaternary paleolake development in the Fen River basin, North China, Geomorphology, 65, 1–13, https://doi.org/10.1016/j.geomorph.2004.06.008, 2005.

Hurtrez, J.-E., Sol, C., and Lucazeau, F.: Effect of drainage area on hypsometry from an analysis of small-scale drainage basins in the Siwalik Hills (Central Nepal), Earth Surface Processes and Landforms, 24, 799–808, https://doi.org/10.1002/(SICI)1096-9837(199908)24:9<799::AID-ESP12>3.0.CO;2-4, 1999a.

Hurtrez, J.-E., Sol, C., and Lucazeau, F.: Effect of drainage area on hypsometry from an analysis of small-scale drainage basins in the Siwalik Hills (Central Nepal), Earth Surface Processes and Landforms, 24, 799–808, https://doi.org/10.1002/(SICI)1096-9837(199908)24:9<799::AID-ESP12>3.0.CO;2-4, 1999b.

Jackson, J. and Leeder, M.: Drainage systems and the development of normal faults: an example from Pleasant Valley, Nevada, Journal of Structural Geology, 16, 1041–1059, https://doi.org/10.1016/0191-8141(94)90051-5, 1994.

Kapp, P., Pullen, A., Pelletier, J. D., Russell, J., Goodman, P., and Cai, F.: From dust to dust: Quaternary wind erosion of the Mu Us Desert and Loess Plateau, China, Geology, 43, 835–838, https://doi.org/10.1130/G36724.1, 2015.

Kattenhorn, S. A., Aydin, A., and Pollard, D. D.: Joints at high angles to normal fault strike: an explanation using 3-D numerical models of fault-perturbed stress fields, Journal of Structural Geology, 22, 1–23, https://doi.org/10.1016/S0191-8141(99)00130-3, 2000.

Kendall, J.-M., Pilidou, S., Keir, D., Bastow, I. D., Stuart, G. W., and Ayele, A.: Mantle upwellings, melt migration and the rifting of Africa: insights from seismic anisotropy, Geological Society, London, Special Publications, 259, 55–72, https://doi.org/10.1144/GSL.SP.2006.259.01.06, 2006.

Kinabo, B. D., Hogan, J. P., Atekwana, E. A., Abdelsalam, M. G., and Modisi, M. P.: Fault growth and propagation during incipient continental rifting: Insights from a combined aeromagnetic and Shuttle Radar Topography Mission digital elevation model investigation of the Okavango Rift Zone, northwest Botswana, Tectonics, 27, https://doi.org/10.1029/2007TC002154, 2008.

Kirby, E. and Whipple, K. X.: Expression of active tectonics in erosional landscapes, Journal of Structural Geology, 44, 54–75, https://doi.org/10.1016/j.jsg.2012.07.009, 2012.

Koehn, D., Aanyu, K., Haines, S., and Sachau, T.: Rift nucleation, rift propagation and the creation of basement micro-plates within active rifts, Tectonophysics, 458, 105–116, https://doi.org/10.1016/j.tecto.2007.10.003, 2008.

Kolawole, F., Atekwana, E. A., Laó-Dávila, D. A., Abdelsalam, M. G., Chindandali, P. R., Salima, J., and Kalindekafe, L.: Active deformation of Malawi rift's north basin Hinge zone modulated by reactivation of preexisting Precambrian Shear zone fabric, Tectonics, 37, 683–704, 2018.

Kolawole, F., Firkins, M. C., Al Wahaibi, T. S., Atekwana, E. A., and Soreghan, M. J.: Rift interaction zones and the stages of rift linkage in active segmented continental rift systems, Basin Research, 33, 2984–3020, 2021a.

Kolawole, F., Phillips, T. B., Atekwana, E. A., and Jackson, C. A.-L.: Structural Inheritance Controls Strain Distribution During Early Continental Rifting, Rukwa Rift, Front. Earth Sci., 9, https://doi.org/10.3389/feart.2021.707869, 2021b.

920   Kolawole, F., Vick, T., Atekwana, E. A., Laó-Dávila, D. A., Costa, A. G., and Carpenter, B. M.: Strain localization and migration during the pulsed lateral propagation of the Shire Rift Zone, East Africa, Tectonophysics, 839, 229499, https://doi.org/10.1016/j.tecto.2022.229499, 2022.

Kolawole, F., Xue, L., and Dulanya, Z.: Rapid Versus Delayed Linkage and Coalescence of Propagating Rift Tips, https://doi.org/10.22541/essoar.168167202.29986035/v2, 4 March 2024.

925   Krabbendam, M. and Barr, T. D.: Proterozoic orogens and the break-up of Gondwana: why did some orogens not rift?, Journal of African Earth Sciences, 31, 35–49, https://doi.org/10.1016/S0899-5362(00)00071-3, 2000.

Kusky, T., Li, J., and Santosh, M.: The Paleoproterozoic North Hebei Orogen: North China craton's collisional suture with the Columbia supercontinent, Gondwana Research, 12, 4–28, https://doi.org/10.1016/j.gr.2006.11.012, 2007.

Kusky, T. M. and Li, J.: Paleoproterozoic tectonic evolution of the North China Craton, Journal of Asian Earth Sciences,
930   22, 383–397, https://doi.org/10.1016/S1367-9120(03)00071-3, 2003.

Lambiase, J. J. and Bosworth, W.: Structural controls on sedimentation in continental rifts, Geological Society, London, Special Publications, 80, 117–144, https://doi.org/10.1144/GSL.SP.1995.080.01.06, 1995.

Leeder, M. R. and Jackson, J. A.: The interaction between normal faulting and drainage in active extensional basins, with examples from the western United States and central Greece, Basin Research, 5, 79–102,
935   https://doi.org/10.1111/j.1365-2117.1993.tb00059.x, 1993.

Leonard, M.: Earthquake Fault Scaling: Self-Consistent Relating of Rupture Length, Width, Average Displacement, and Moment Release, Bulletin of the Seismological Society of America, 100, 1971–1988, https://doi.org/10.1785/0120090189, 2010.

Lezzar, K. E., Tiercelin, J.-J., Le Turdu, C., Cohen, Andrew. S., Reynolds, D. J., Le Gall, B., and Scholz, C. A.: Control of
940   Normal Fault Interaction on the Distribution of Major Neogene Sedimentary Depocenters, Lake Tanganyika, East African Rift, AAPG Bulletin, 86, 1027–1059, https://doi.org/10.1306/61EEDC1A-173E-11D7-8645000102C1865D, 2002.

Li, S., Zhao, G., Wilde, S. A., Zhang, J., Sun, M., Zhang, G., and Dai, L.: Deformation history of the Hengshan–Wutai–Fuping Complexes: Implications for the evolution of the Trans-North China Orogen, Gondwana Research, 18,
945   611–631, https://doi.org/10.1016/j.gr.2010.03.003, 2010.

Li, Y., Yang, J., Xia, Z., and Mo, D.: Tectonic geomorphology in the Shanxi Graben System, northern China, Geomorphology, 23, 77–89, https://doi.org/10.1016/S0169-555X(97)00092-5, 1998.

Lifton, N. A. and Chase, C. G.: Tectonic, climatic and lithologic influences on landscape fractal dimension and hypsometry: implications for landscape evolution in the San Gabriel Mountains, California, Geomorphology, 5, 77–114,
950   https://doi.org/10.1016/0169-555X(92)90059-W, 1992.

Maerten, L.: Variation in slip on intersecting normal faults: Implications for paleostress inversion, Journal of Geophysical Research: Solid Earth, 105, 25553–25565, https://doi.org/10.1029/2000JB900264, 2000.

Makrari, S., Sharma, G., Taloor, A. K., Singh, M. S., Sarma, K. K., and Aggarwal, S. P.: Assessment of the geomorphic indices in relation to tectonics along selected sectors of Borpani River Basin, Assam using Cartosat DEM data, Geosystems and Geoenvironment, 1, 100068, https://doi.org/10.1016/j.geogeo.2022.100068, 2022.

Masek, J. G., Isacks, B. L., Gubbels, T. L., and Fielding, E. J.: Erosion and tectonics at the margins of continental plateaus, Journal of Geophysical Research: Solid Earth, 99, 13941–13956, https://doi.org/10.1029/94JB00461, 1994.

McCaffrey, K. J. W.: Controls on reactivation of a major fault zone: the Fair Head–Clew Bay line in Ireland, Journal of the Geological Society, 154, 129–133, https://doi.org/10.1144/gsjgs.154.1.0129, 1997.

Menzies, M., Xu, Y., Zhang, H., and Fan, W.: Integration of geology, geophysics and geochemistry: A key to understanding the North China Craton, Lithos, 96, 1–21, https://doi.org/10.1016/j.lithos.2006.09.008, 2007.

Menzies, M. A. and Xu, Y.: Geodynamics of the North China Craton, in: Mantle Dynamics and Plate Interactions in East Asia, American Geophysical Union (AGU), 155–165, https://doi.org/10.1029/GD027p0155, 1998.

Menzies, M. A., Fan, W., and Zhang, M.: Palaeozoic and Cenozoic lithoprobes and the loss of >120 km of Archaean lithosphere, Sino-Korean craton, China, Geological Society, London, Special Publications, 76, 71–81, https://doi.org/10.1144/GSL.SP.1993.076.01.04, 1993.

Middleton, T. A., Elliott, J. R., Rhodes, E. J., Sherlock, S., Walker, R. T., Wang, W., Yu, J., and Zhou, Y.: Extension rates across the northern Shanxi Grabens, China, from Quaternary geology, seismicity and geodesy, Geophysical Journal International, 209, 535–558, 2017.

Molnar, N., Cruden, A., and Betts, P.: The role of inherited crustal and lithospheric architecture during the evolution of the Red Sea: Insights from three dimensional analogue experiments, Earth and Planetary Science Letters, 544, 116377, https://doi.org/10.1016/j.epsl.2020.116377, 2020.

Moore, J. M. and Davidson, A.: Rift structure in southern Ethiopia, Tectonophysics, 46, 159–173, https://doi.org/10.1016/0040-1951(78)90111-7, 1978.

Morley, C. K.: Variable extension in Lake Tanganyika, Tectonics, 7, 785–801, https://doi.org/10.1029/TC007i004p00785, 1988.

Morley, C. K.: Stress re-orientation along zones of weak fabrics in rifts: An explanation for pure extension in 'oblique' rift segments?, Earth and Planetary Science Letters, 297, 667–673, https://doi.org/10.1016/j.epsl.2010.07.022, 2010.

Morley, C. K., Nelson, R. A., Patton, T. L., and Munn, S. G.: Transfer Zones in the East African Rift System and Their Relevance to Hydrocarbon Exploration in Rifts1, AAPG Bulletin, 74, 1234–1253, https://doi.org/10.1306/0C9B2475-1710-11D7-8645000102C1865D, 1990.

Morley, C. K., Haranya, C., Phoosongsee, W., Pongwapee, S., Kornsawan, A., and Wonganan, N.: Activation of rift oblique and rift parallel pre-existing fabrics during extension and their effect on deformation style: examples from the rifts of Thailand, Journal of Structural Geology, 26, 1803–1829, https://doi.org/10.1016/j.jsg.2004.02.014, 2004.

985 Mulaya, E., Gluyas, J., McCaffrey, K., Phillips, T., and Ballentine, C.: Structural geometry and evolution of the Rukwa Rift Basin, Tanzania: Implications for helium potential, Basin Research, 34, 938–960, https://doi.org/10.1111/bre.12646, 2022.

Musila, M., Ebinger, C. J., Bastow, I. D., Sullivan, G., Oliva, S. J., Knappe, E., Perry, M., Kounoudis, R., Ogden, C. S., Bendick, R., Mwangi, S., Mariita, N., Kianji, G., Kraus, E., and Illsley-Kemp, F.: Active Deformation Constraints

990 on the Nubia-Somalia Plate Boundary Through Heterogenous Lithosphere of the Turkana Depression, Geochemistry, Geophysics, Geosystems, 24, e2023GC010982, https://doi.org/10.1029/2023GC010982, 2023.

Nelson, R. A., Patton, T. L., and Morley, C. K.: Rift-Segment Interaction and Its Relation to Hydrocarbon Exploration in Continental Rift Systems (1), AAPG Bulletin, 76, 1153–1169, 1992.

Obaid, A. K. and Allen, M. B.: Landscape expressions of tectonics in the Zagros fold-and-thrust belt, Tectonophysics, 766,

995 20–30, https://doi.org/10.1016/j.tecto.2019.05.024, 2019.

Osagiede, E. E., Rotevatn, A., Gawthorpe, R., Kristensen, T. B., Jackson, C. A.-L., and Marsh, N.: Pre-existing intra-basement shear zones influence growth and geometry of non-colinear normal faults, western Utsira High–Heimdal Terrace, North Sea, Journal of Structural Geology, 130, 103908, https://doi.org/10.1016/j.jsg.2019.103908, 2020.

Pavlides, S. B., Zouros, N. C., Zhongjing, F., Shaoping, C., Tranos, M. D., and Chatzipetros, A. A.: Geometry, kinematics

1000 and morphotectonics of the Yanqing–Huailai active faults (northern China), Tectonophysics, 308, 99–118, https://doi.org/10.1016/S0040-1951(99)00074-8, 1999.

Peace, A., McCaffrey, K., Imber, J., Hunen, J. van, Hobbs, R., and Wilson, R.: The role of pre-existing structures during rifting, continental breakup and transform system development, offshore West Greenland, Basin Research, 30, 373–394, https://doi.org/10.1111/bre.12257, 2018.

1005 Pérez-Peña, J. V., Azañón, J. M., Booth-Rea, G., Azor, A., and Delgado, J.: Differentiating geology and tectonics using a spatial autocorrelation technique for the hypsometric integral, Journal of Geophysical Research: Earth Surface, 114, https://doi.org/10.1029/2008JF001092, 2009.

Perron, J. T. and Royden, L.: An integral approach to bedrock river profile analysis, Earth Surface Processes and Landforms, 38, 570–576, https://doi.org/10.1002/esp.3302, 2013.

1010 Petit, C., Deverchere, J., Houdry, F., Sankov, V. A., Melnikova, V. I., and Delvaux, D.: Present-day stress field changes along the Baikal rift and tectonic implications, Tectonics, 15, 1171–1191, 1996.

Philippon, M., Willingshofer, E., Sokoutis, D., Corti, G., Sani, F., Bonini, M., and Cloetingh, S.: Slip re-orientation in oblique rifts, Geology, 43, 147–150, 2015.

Phillips, T. B. and McCaffrey, K. J. W.: Terrane Boundary Reactivation, Barriers to Lateral Fault Propagation and

1015 Reactivated Fabrics: Rifting Across the Median Batholith Zone, Great South Basin, New Zealand, Tectonics, 38, 4027–4053, https://doi.org/10.1029/2019TC005772, 2019.

Phillips, T. B., Jackson, C. A., Bell, R. E., Duffy, O. B., and Fossen, H.: Reactivation of intrabasement structures during rifting: A case study from offshore southern Norway, Journal of Structural Geology, 91, 54–73, 2016.

Phillips, T. B., Naliboff, J. B., McCaffrey, K. J. W., Pan, S., van Hunen, J., and Froemchen, M.: The influence of crustal

1020   strength on rift geometry and development – insights from 3D numerical modelling, Solid Earth, 14, 369–388, https://doi.org/10.5194/se-14-369-2023, 2023.

Qi, J. and Yang, Q.: Cenozoic structural deformation and dynamic processes of the Bohai Bay basin province, China, Marine and Petroleum Geology, 27, 757–771, https://doi.org/10.1016/j.marpetgeo.2009.08.012, 2010.

Ramos, G. V., Vasconcelos, D. L., Marques, F. O., de Castro, D. L., Nogueira, F. C. C., Bezerra, F. H. R., Perez, Y. A. R.,

1025   Souza, J. A. B., and Medeiros, V. C.: Relations between inherited basement fabric and fault nucleation in a continental setting: The Rio do Peixe Basin, NE Brazil, Marine and Petroleum Geology, 139, 105635, https://doi.org/10.1016/j.marpetgeo.2022.105635, 2022.

Reeve, M. T., Bell, R. E., Duffy, O. B., Jackson, C. A.-L., and Sansom, E.: The growth of non-colinear normal fault systems; What can we learn from 3D seismic reflection data?, Journal of Structural Geology, 70, 141–155, 2015.

1030   Ring, U.: The influence of preexisting structure on the evolution of the Cenozoic Malawi rift (East African rift system), Tectonics, 13, 313–326, https://doi.org/10.1029/93TC03188, 1994.

Rosendahl, B. R.: Architecture of Continental Rifts with Special Reference to East Africa, Annual Review of Earth and Planetary Sciences, 15, 445–503, https://doi.org/10.1146/annurev.ea.15.050187.002305, 1987.

Rotevatn, A., Kristensen, T. B., Ksienzyk, A. K., Wemmer, K., Henstra, G. A., Midtkandal, I., Grundvåg, S.-A., and

1035   Andresen, A.: Structural Inheritance and Rapid Rift-Length Establishment in a Multiphase Rift: The East Greenland Rift System and its Caledonian Orogenic Ancestry, Tectonics, 37, 1858–1875, https://doi.org/10.1029/2018TC005018, 2018.

Sachau, T., Koehn, D., Stamps, D. S., and Lindenfeld, M.: Fault kinematics and stress fields in the Rwenzori Mountains, Uganda, Int J Earth Sci (Geol Rundsch), 105, 1729–1740, https://doi.org/10.1007/s00531-015-1162-6, 2016.

1040   Samsu, A., Cruden, A. R., Micklethwaite, S., Grose, L., and Vollgger, S. A.: Scale matters: The influence of structural inheritance on fracture patterns, Journal of Structural Geology, 130, 103896, https://doi.org/10.1016/j.jsg.2019.103896, 2020.

Samsu, A., Micklethwaite, S., Williams, J. N., Fagereng, Å., and Cruden, A. R.: Structural inheritance in amagmatic rift basins: Manifestations and mechanisms for how pre-existing structures influence rift-related faults, Earth-Science

1045   Reviews, 246, 104568, https://doi.org/10.1016/j.earscirev.2023.104568, 2023.

Santosh, M.: Assembling North China Craton within the Columbia supercontinent: The role of double-sided subduction, Precambrian Research, 178, 149–167, https://doi.org/10.1016/j.precamres.2010.02.003, 2010.

Schiffer, C., Doré, A. G., Foulger, G. R., Franke, D., Geoffroy, L., Gernigon, L., Holdsworth, B., Kusznir, N., Lundin, E., McCaffrey, K., Peace, A. L., Petersen, K. D., Phillips, T. B., Stephenson, R., Stoker, M. S., and Welford, J. K.:

1050   Structural inheritance in the North Atlantic, Earth-Science Reviews, 206, 102975, https://doi.org/10.1016/j.earscirev.2019.102975, 2020.

Schmidt, K. M. and Montgomery, D. R.: Limits to Relief, Science, 270, 617–620, https://doi.org/10.1126/science.270.5236.617, 1995.

Scholz, C. A.: Deltas of the Lake Malawi Rift, East Africa: Seismic Expression and Exploration Implications 1, AAPG Bulletin, 79, 1679–1697, https://doi.org/10.1306/7834DE54-1721-11D7-8645000102C1865D, 1995.

Scholz, C. H.: Scaling laws for large earthquakes: Consequences for physical models, Bulletin of the Seismological Society of America, 72, 1–14, https://doi.org/10.1785/BSSA0720010001, 1982.

Schumacher, M. E.: Upper Rhine Graben: Role of preexisting structures during rift evolution, Tectonics, 21, 6-1-6–17, https://doi.org/10.1029/2001TC900022, 2002.

Schwanghart, W. and Scherler, D.: Short Communication: TopoToolbox 2 – MATLAB-based software for topographic analysis and modeling in Earth surface sciences, Earth Surface Dynamics, 2, 1–7, https://doi.org/10.5194/esurf-2-1-2014, 2014.

Şengör, A. M. C., Lom, N., and Sağdıç, N. G.: Tectonic inheritance, structure reactivation and lithospheric strength: the relevance of geological history, Geological Society, London, Special Publications, 470, 105–136, https://doi.org/10.1144/SP470.8, 2019.

Shanxi Bureau of Geology and Mineral Resources (SBGMR): Regional Geology of Shanxi Province, Geological Publishing House, Beijing, China, 1989.

Shen, Z.-K., Zhao, C., Yin, A., Li, Y., Jackson, D. D., Fang, P., and Dong, D.: Contemporary crustal deformation in east Asia constrained by Global Positioning System measurements, Journal of Geophysical Research: Solid Earth, 105, 5721–5734, https://doi.org/10.1029/1999JB900391, 2000.

Shi, W., Dong, S., Liu, Y., Hu, J., Chen, X., and Chen, P.: Cenozoic tectonic evolution of the South Ningxia region, northeastern Tibetan Plateau inferred from new structural investigations and fault kinematic analyses, Tectonophysics, 649, 139–164, https://doi.org/10.1016/j.tecto.2015.02.024, 2015a.

Shi, W., Cen, M., Chen, L., Wang, Y., Chen, X., Li, J., and Chen, P.: Evolution of the late Cenozoic tectonic stress regime in the Shanxi Rift, central North China Plate inferred from new fault kinematic analysis, Journal of Asian Earth Sciences, 114, 54–72, https://doi.org/10.1016/j.jseaes.2015.04.044, 2015b.

Shi, W., Dong, S., and Hu, J.: Neotectonics around the Ordos Block, North China: A review and new insights, Earth-Science Reviews, 200, 102969, 2020.

Snyder, N. P., Whipple, K. X., Tucker, G. E., and Merritts, D. J.: Landscape response to tectonic forcing: Digital elevation model analysis of stream profiles in the Mendocino triple junction region, northern California, Geological Society of America Bulletin, 112, 1250–1263, 2000.

Storchak, D. A., Di Giacomo, D., Bondar, I., Engdahl, E. R., Harris, J., Lee, W. H. K., Villasenor, A., and Bormann, P.: Public Release of the ISC-GEM Global Instrumental Earthquake Catalogue (1900-2009), Seismological Research Letters, 84, 810–815, https://doi.org/10.1785/0220130034, 2013.

1085   Storchak, D. A., Di Giacomo, D., Engdahl, E. R., Harris, J., Bondár, I., Lee, W. H., Bormann, P., and Villaseñor, A.: The ISC-GEM global instrumental earthquake catalogue (1900–2009): introduction, Physics of the Earth and Planetary Interiors, 239, 48–63, 2015.

Strahler, A. N.: Hypsometirc (area-altitude) Analysis of erosional topography, GSA Bulletin, 63, 1117–1142, https://doi.org/10.1130/0016-7606(1952)63[1117:HAAOET]2.0.CO;2, 1952.

1090   Strahler, A. N.: Quantitative analysis of watershed geomorphology, Eos, Transactions American Geophysical Union, 38, 913–920, https://doi.org/10.1029/TR038i006p00913, 1957.

Su, P., He, H., Tan, X., Liu, Y., Shi, F., and Kirby, E.: Initiation and evolution of the Shanxi Rift System in North China: Evidence from low-temperature thermochronology in a plate reconstruction framework, Tectonics, 40, e2020TC006298, 2021.

1095   Su, P., He, H., Liu, Y., Shi, F., Granger, D. E., Kirby, E., Luo, L., Han, F., and Lu, R.: Quantifying the Structure and Extension Rate of the Linfen Basin, Shanxi Rift System Since the Latest Miocene: Implications for Continental Magma-Poor Rifting, Tectonics, 42, e2023TC007885, https://doi.org/10.1029/2023TC007885, 2023.

Tang Y.-C., Fen Y.-G., Chen Zhongshun J., Zhou S.-Y., Ning J.-Y., Wei S.-Q., Li P., Chun-Quan Y., Fan W.-Y., and Wang H.-Y.: Receiver function analysis at Shanxi Rift, Chinese Journal of Geophysics, 53, 2102–2109,

1100   https://doi.org/10.3969/j.issn.0001-5733.2010.09.010, 2010.

Taylor, S. K., Bull, J. M., Lamarche, G., and Barnes, P. M.: Normal fault growth and linkage in the Whakatane Graben, New Zealand, during the last 1.3 Myr, Journal of Geophysical Research: Solid Earth, 109, https://doi.org/10.1029/2003JB002412, 2004.

Tepp, G., Ebinger, C. J., Zal, H., Gallacher, R., Accardo, N., Shillington, D. J., Gaherty, J., Keir, D., Nyblade, A. A.,

1105   Mbogoni, G. J., Chindandali, P. R. N., Ferdinand-Wambura, R., Mulibo, G. D., and Kamihanda, G.: Seismic Anisotropy of the Upper Mantle Below the Western Rift, East Africa, Journal of Geophysical Research: Solid Earth, 123, 5644–5660, https://doi.org/10.1029/2017JB015409, 2018.

Tommasi, A. and Vauchez, A.: Continental rifting parallel to ancient collisional belts: an effect of the mechanical anisotropy of the lithospheric mantle, Earth and Planetary Science Letters, 185, 199–210,

1110   https://doi.org/10.1016/S0012-821X(00)00350-2, 2001.

Trap, P., Faure, M., Lin, W., and Monié, P.: Late Paleoproterozoic (1900–1800Ma) nappe stacking and polyphase deformation in the Hengshan–Wutaishan area: Implications for the understanding of the Trans-North-China Belt, North China Craton, Precambrian Research, 156, 85–106, https://doi.org/10.1016/j.precamres.2007.03.001, 2007.

Trap, P., Faure, M., Lin, W., Bruguier, O., and Monié, P.: Contrasted tectonic styles for the Paleoproterozoic evolution of

1115   the North China Craton. Evidence for a ~2.1Ga thermal and tectonic event in the Fuping Massif, Journal of Structural Geology, 30, 1109–1125, https://doi.org/10.1016/j.jsg.2008.05.001, 2008.

Trap, P., Faure, M., Lin, W., and Meffre, S.: The Lüliang Massif: a key area for the understanding of the Palaeoproterozoic Trans-North China Belt, North China Craton, Geological Society, London, Special Publications, 323, 99–125, 2009a.

1120 Trap, P., Faure, M., Lin, W., Monié, P., Meffre, S., and Melleton, J.: The Zanhuang Massif, the second and eastern suture zone of the Paleoproterozoic Trans-North China Orogen, Precambrian Research, 172, 80–98, 2009b.

Trap, P., Faure, M., Lin, W., Le Breton, N., and Monié, P.: Paleoproterozoic tectonic evolution of the Trans-North China Orogen: Toward a comprehensive model, Precambrian Research, 222–223, 191–211, https://doi.org/10.1016/j.precamres.2011.09.008, 2012.

1125 Vasconcelos, D. L., Bezerra, F. H. R., Medeiros, W. E., de Castro, D. L., Clausen, O. R., Vital, H., and Oliveira, R. G.: Basement fabric controls rift nucleation and postrift basin inversion in the continental margin of NE Brazil, Tectonophysics, 751, 23–40, https://doi.org/10.1016/j.tecto.2018.12.019, 2019.

Vauchez, A., Barruol, G., and Tommasi, A.: Why do continents break-up parallel to ancient orogenic belts?, Terra Nova, 9, 62–66, https://doi.org/10.1111/j.1365-3121.1997.tb00003.x, 1997.

1130 Versfelt, J. and Rosendahl, B. R.: Relationships between pre-rift structure and rift architecture in Lakes Tanganyika and Malawi, East Africa, Nature, 337, 354–357, https://doi.org/10.1038/337354a0, 1989.

Vetel, W. and Le Gall, B.: Dynamics of prolonged continental extension in magmatic rifts: the Turkana Rift case study (North Kenya), Geological Society, London, Special Publications, 259, 209–233, https://doi.org/10.1144/GSL.SP.2006.259.01.17, 2006.

1135 Walcott, R. C. and Summerfield, M. A.: Scale dependence of hypsometric integrals: An analysis of southeast African basins, Geomorphology, 96, 174–186, https://doi.org/10.1016/j.geomorph.2007.08.001, 2008.

Wedmore, L. N. J., Williams, J. N., Biggs, J., Fagereng, Å., Mphepo, F., Dulanya, Z., Willoughby, J., Mdala, H., and Adams, B. A.: Structural inheritance and border fault reactivation during active early-stage rifting along the Thyolo fault, Malawi, Journal of Structural Geology, 139, 104097, https://doi.org/10.1016/j.jsg.2020.104097,
1140 2020.

Wedmore, L. N. J., Turner, T., Biggs, J., Williams, J. N., Sichingabula, H. M., Kabumbu, C., and Banda, K.: The Luangwa Rift Active Fault Database and fault reactivation along the southwestern branch of the East African Rift, Solid Earth, 13, 1731–1753, https://doi.org/10.5194/se-13-1731-2022, 2022.

Wheeler, W. H. and Karson, J. A.: Structure and kinematics of the Livingstone Mountains border fault zone, Nyasa
1145 (Malawi) Rift, southwestern Tanzania, Journal of African Earth Sciences (and the Middle East), 8, 393–413, https://doi.org/10.1016/S0899-5362(89)80034-X, 1989.

Whipple, K. X.: Bedrock rivers and the geomorphology of active orogens, Annu. Rev. Earth Planet. Sci., 32, 151–185, https://doi.org/10.1146/annurev.earth.32.101802.120356, 2004.

Whittaker, A. C.: How do landscapes record tectonics and climate?, Lithosphere, 4, 160–164, 2012.

1150 Whittaker, A. C. and Walker, A. S.: Geomorphic constraints on fault throw rates and linkage times: Examples from the
         Northern Gulf of Evia, Greece, Journal of Geophysical Research: Earth Surface, 120, 137–158,
         https://doi.org/10.1002/2014JF003318, 2015.

Whittaker, A. C., Attal, M., Cowie, P. A., Tucker, G. E., and Roberts, G.: Decoding temporal and spatial patterns of fault
         uplift using transient river long profiles, Geomorphology, 100, 506–526,
1155   https://doi.org/10.1016/j.geomorph.2008.01.018, 2008.

Williams, J. N., Fagereng, Å., Wedmore, L. N., Biggs, J., Mphepo, F., Dulanya, Z., Mdala, H., and Blenkinsop, T.: How do
         variably striking faults reactivate during rifting? Insights from southern Malawi, Geochemistry, Geophysics,
         Geosystems, 20, 3588–3607, 2019.

Wilson, J. T.: Did the Atlantic Close and then Re-Open?, Nature, 211, 676–681, https://doi.org/10.1038/211676a0, 1966.

1160 Wilson, R. W., Holdsworth, R. E., Wild, L. E., McCaffrey, K. J. W., England, R. W., Imber, J., and Strachan, R. A.:
         Basement-influenced rifting and basin development: a reappraisal of post-Caledonian faulting patterns from the
         North Coast Transfer Zone, Scotland, Geological Society, London, Special Publications, 335, 795–826,
         https://doi.org/10.1144/SP335.32, 2010.

Wobus, C., Whipple, K. X., Kirby, E., Snyder, N., Johnson, J., Spyropolou, K., Crosby, B., and Sheehan, D.: Tectonics
1165   from topography: Procedures, promise, and pitfalls, in: Tectonics, Climate, and Landscape Evolution, vol. 398,
         edited by: Willett, S. D., Hovius, N., Brandon, M. T., and Fisher, D. M., Geological Society of America, 0,
         https://doi.org/10.1130/2006.2398(04), 2006.

Wong, W. H.: Crustal Movements and Igneous Activities in Eastern China Since Mesozoic Time.1, Bulletin of the
         Geological Society of China, 6, 9–37, https://doi.org/10.1111/j.1755-6724.1927.mp6001002.x, 1927.

1170 Xu, X. and Ma, X.: Geodynamics of the Shanxi rift system, China, Tectonophysics, 208, 325–340, 1992.

Xu, X., Ma, X., and Deng, Q.: Neotectonic activity along the Shanxi rift system, China, Tectonophysics, 219, 305–325,
         1993.

Xu, Y., He, H., Deng, Q., Allen, M. B., Sun, H., and Bi, L.: The CE 1303 Hongdong Earthquake and the Huoshan Piedmont
         Fault, Shanxi Graben: Implications for Magnitude Limits of Normal Fault Earthquakes, J. Geophys. Res. Solid
1175   Earth, 123, 3098–3121, https://doi.org/10.1002/2017JB014928, 2018.

Yin, A.: Cenozoic tectonic evolution of Asia: A preliminary synthesis, Tectonophysics, 488, 293–325,
         https://doi.org/10.1016/j.tecto.2009.06.002, 2010.

Zhai, M., Li, T.-S., Peng, P., Hu, B., Liu, F., and Zhang, Y.: Precambrian key tectonic events and evolution of the North
         China craton, https://doi.org/10.1144/SP338.12, 2010.

1180 Zhai, M.-G. and Santosh, M.: The early Precambrian odyssey of the North China Craton: A synoptic overview, Gondwana
         Research, 20, 6–25, https://doi.org/10.1016/j.gr.2011.02.005, 2011.

Zhang, C., Li, C., Deng, H., Liu, Y., Liu, L., Wei, B., Li, H., and Liu, Z.: Mesozoic contraction deformation in the Yanshan and northern Taihang mountains and its implications to the destruction of the North China Craton, Sci. China Earth Sci., 54, 798–822, https://doi.org/10.1007/s11430-011-4180-7, 2011.

Zhang, Y., Ma, Y., Yang, N., Shi, W., and Dong, S.: Cenozoic extensional stress evolution in North China, Journal of Geodynamics, 36, 591–613, https://doi.org/10.1016/j.jog.2003.08.001, 2003.

Zhang, Y., Dong, S., Zhao, Y., and Zhang, T.: Jurassic Tectonics of North China: A Synthetic View, Acta Geologica Sinica - English Edition, 82, 310–326, https://doi.org/10.1111/j.1755-6724.2008.tb00581.x, 2008.

Zhang, Y. Q., Mercier, J. L., and Vergély, P.: Extension in the graben systems around the Ordos (China), and its contribution to the extrusion tectonics of south China with respect to Gobi-Mongolia, Tectonophysics, 285, 41–75, https://doi.org/10.1016/S0040-1951(97)00170-4, 1998.

Zhao, G., Min, S., Wilde, S. A., and Sanzhong, L.: Late Archean to Paleoproterozoic evolution of the North China Craton: key issues revisited, Precambrian Research, 136, 177–202, https://doi.org/10.1016/j.precamres.2004.10.002, 2005.

Zhao, L. and Zheng, T.: Using shear wave splitting measurements to investigate the upper mantle anisotropy beneath the North China Craton: Distinct variation from east to west, Geophysical Research Letters, 32, https://doi.org/10.1029/2005GL022585, 2005.

Zhu, R., Xu, Y., Zhu, G., Zhang, H., Xia, Q., and Zheng, T.: Destruction of the North China Craton, Sci. China Earth Sci., 55, 1565–1587, https://doi.org/10.1007/s11430-012-4516-y, 2012.

Ziegler, P. A. and Cloetingh, S.: Dynamic processes controlling evolution of rifted basins, Earth-Science Reviews, 64, 1–50, https://doi.org/10.1016/S0012-8252(03)00041-2, 2004.

Zwaan, F. and Schreurs, G.: How oblique extension and structural inheritance influence rift segment interaction: Insights from 4D analog models, Interpretation, 5, SD119–SD138, https://doi.org/10.1190/INT-2016-0063.1, 2017.

Zwaan, F., Schreurs, G., Naliboff, J., and Buiter, S. J. H.: Insights into the effects of oblique extension on continental rift interaction from 3D analogue and numerical models, Tectonophysics, 693, 239–260, https://doi.org/10.1016/j.tecto.2016.02.036, 2016.

Zwaan, F., Chenin, P., Erratt, D., Manatschal, G., and Schreurs, G.: Competition between 3D structural inheritance and kinematics during rifting: Insights from analogue models, Basin Research, 34, 824–854, https://doi.org/10.1111/bre.12642, 2022.